

# Coherent Parity Check Construction for Quantum Error Correction

Nicholas Chancellor<sup>1\*</sup>, Aleks Kissinger<sup>2</sup>, Stefan Zohren<sup>3†</sup>,  
Dominic Horsman<sup>1‡</sup>

<sup>1</sup>*Department of Physics, Durham University, South Road,  
Durham DH1 3LE, UK*

<sup>2</sup>*Department of Computer Science, Nijmegen University,  
Nijmegen, Netherlands*

<sup>3</sup>*Department of Material Science, and  
Advanced Research Computing, University of Oxford  
Parks Road, Oxford OX1 3PH, UK*

Tuesday 14<sup>th</sup> June, 2022

## Abstract

We present a framework for constructing and analysing quantum error correction codes that gives simple and intuitive tools for designing codes based on device specifications. Built from a direct analog of classical parity checking, these coherent parity codes use a simple model for constraints between qubits and decoding of information. With an associated graphical language, this coherent parity check (CPC) construction enables automated search for codes, and we give discovered examples of low-overhead codes for small devices ( $[[10,3,3]]$ , and  $[[12,4,3]]$ ) based on realistic error rates taken from current ion trap state-of-the-art. We show that CPC codes form a class of CSS codes. We further show that the graphical language maps to the category-theoretic ZX calculus, which enables the use of the automated reasoning tool Quantomatic to derive properties of the codes. We show how automated reasoning allows us to perform computation between qubits in the same code-block without requiring multiple codeblocks and/or transversal gates. These tools offer a significant aid to put quantum error correction theory into design practice for practical quantum technologies in both the immediate future and looking forwards to large-scale deployable quantum computing. Furthermore, the close theoretical link between the CPC construction and classical error correction codes opens up the possibility of constructing quantum versions of modern high-performance error correction codes (such as LDPC and turbo codes) that approach the Shannon limit.

---

\*nicholas.chancellor@durham.ac.uk

†stefan.zohren@materials.ox.ac.uk

‡dominic.horsman@durham.ac.uk

# Contents

<b>1</b>	<b>Introduction</b>	<b>3</b>
<b>2</b>	<b>Coherent bit-flip correction codes</b>	<b>6</b>
2.1	A two qubit coherent parity check . . . . .	7
2.2	Three qubit bit-flip error correction . . . . .	9
2.3	Numerical performance of the $[[6, 3, 1]]$ code in ion traps . . . . .	14
2.4	Stabilizers and the bit-flip code . . . . .	16
2.5	Review of Formalism for Decoding Classical Parity Codes . . . . .	17
<b>3</b>	<b>Tools for constructing full CPC codes</b>	<b>18</b>
3.1	Graphical tools for parity codes . . . . .	19
3.2	Effective classical parity codes . . . . .	22
3.3	Proof of Graphical Formalism for Propagation . . . . .	23
<b>4</b>	<b>Full CPC codes to correct single errors</b>	<b>25</b>
4.1	Two small quantum parity codes . . . . .	25
4.2	Numerical tests of $[[11, 3, 3]]$ and $[[12, 4, 3]]$ codes . . . . .	27
<b>5</b>	<b>Combining bit-flip and phase checks</b>	<b>28</b>
5.1	Graphical rules for general parity checks . . . . .	29
5.2	Turning the $[[11, 3, 3]]$ code into $[[10, 3, 3]]$ . . . . .	31
5.3	Proof of the more general graphical formalism . . . . .	33
<b>6</b>	<b>CPC codes and stabilizer codes</b>	<b>34</b>
6.1	Stabilizers for separable CPC codes . . . . .	34
6.2	Stabilizers in the More General Formalism . . . . .	36
6.3	Relationship to CSS codes . . . . .	36
<b>7</b>	<b>Continuous protection for quantum memories</b>	<b>38</b>
7.1	Protecting during encode and decode . . . . .	38
7.2	Asynchronous error checking . . . . .	40
<b>8</b>	<b>Computation encoded in error correction cycles</b>	<b>41</b>
8.1	Single qubit operations . . . . .	41
8.2	Entangling gates: encoded CNOT . . . . .	42
8.3	Multiple operations per cycle . . . . .	45
<b>9</b>	<b>Explicit calculation of CPC codes in Quantomatic</b>	<b>45</b>
<b>10</b>	<b>Outlook and conclusions</b>	<b>53</b>
10.1	Scaling for CPC codes . . . . .	54
10.2	Thresholds . . . . .	54
10.3	Future directions . . . . .	55
	<b>Bibliography</b>	<b>60</b>

# 1 Introduction

Quantum information processing is a computing revolution in progress. It depends, however, on a delicate balancing act: qubits (quantum bits) are fragile and need to be protected from noise from the environment, but also need to interact strongly in order to produce superposed states and quantum entanglement. The solution is to use quantum error correction codes, a breakthrough that enabled the development of quantum computing as a viable future technology. Since the original discovery (Shor, 1995; Calderbank and Shor, 1996; Knill et al., 1996; Aharonov and Ben-Or, 1996; Steane, 1996b; Laflamme et al., 1996; Steane, 1996a) that error correction for quantum systems is possible, a wide variety of codes covering various quantum architectures, including the circuit model and measurement-based quantum computing, have appeared. See e.g. (Gottesman, 2010) for an overview. More recent developments include topological surface and color codes (Kitaev, 2003; Raussendorf et al., 2007; Raussendorf and Harrington, 2007; Dennis et al., 2002; Bombin and Martin-Delgado, 2008), and extensions to higher dimensions (Campbell, 2014).

Many quantum error correction codes protect one logical qubit at a time by using the redundancy of encoding the information into a larger number of qubits. This provides simplicity in terms of encoding and decoding, as well as in the design of fault-tolerant computations, but quickly incurs overheads that are impractical for emerging, small-scale devices. A notable exception are CSS codes, which turn a pair of classical error correcting codes satisfying a particular property into one quantum error correcting code (Calderbank and Shor, 1996). These are significantly more efficient, but finding such codes and associated fault-tolerant computation schemes can be complicated. The latter are also restrictive, in that they typically focus only on *transversal* sets of gates (Easton and Knill, 2009), where two-qubit operations can only be implemented between distinct code blocks.

With the imminent arrival of first-generation quantum computers (e.g. (O’Malley et al., 2016; , n.d.; Nickerson et al., 2014)), tailoring of error correction codes to the particular architecture, error model, connectivity, and resource requirements of individual devices becomes a key challenge. Quantum error correction theory has tended towards a ‘one-size-fits-all’ approach. The practicalities of constructing quantum technologies means a much more customised and flexible approach will be needed. Furthermore, the large resources of classical high-performance error correction remains largely untapped. For example, while some progress has been made in building quantum error correcting codes from classical low-density parity codes (LDPCs) (MacKay et al., 2004), these techniques impose severe restrictions on the types of classical codes that can be used. LDPCs were first introduced in (Gallager, 1962, 1963), and more recently (MacKay and Neal, 1996; MacKay, 1999) shown to have performance close to the Shannon limit. This makes them competitive with other state-of-the-art codes such as turbo codes (Berrou et al., 1993; Berrou and Glavieux, 1996), which also have no current quantum analog. (We refer the reader to (MacKay, 2003) for a textbook account giving an excellent overview of classical error correction.)

Part of the problem behind expanding the space of quantum codes and customising them to hardware is the obvious difficulty of simulating them on current, classical, computers. They are by definition systems undergoing quantum evolution. Topologi-

cal codes use notions of braiding and homology to give large-scale descriptions of their operation. These tend not to be of much use to fine-tune the implementation of these codes on specific devices. CSS codes have no high-level language, and their previous definition in terms of pairs of classical codes satisfying specific properties was explicitly non-constructive.

In this paper we give a new framework for constructing quantum CSS stabilizer codes that will address these deficiencies. Based on the fundamental gadget of the *coherent parity check* (CPC), this construction shows that error correction can be modelled as a set of constraints between data and parity-check qubits (for both bit and phase), in straightforward analogy with classical parity checking. This construction comes with an associated graphical language that is easy to use and to program, making it a powerful tool to search the space of quantum codes. We give explicit constructions for small-scale codes showing how the new framework functions as a design tool. The way the framework is constructed with reference to classical parity checks makes translation to and from classical codes clear and intuitive. Furthermore, the graphical language is supported by an existing software package for the ZX calculus based on a category-theoretic construction of quantum mechanics. This gives support to the construction as a high-level formal language for quantum stabilizer codes, suitable for both directed and automated code search, development, and customisation.

The fundamental element of the CPC construction is the coherent parity check itself. Quantum error correction as it is usually formulated is based on encoding  $n$  logical qubits into  $N$  physical qubits, with  $N - n$  known stabilizer operators. These are measured to produce syndromes, without affecting the logical subspaces into which the logical qubits are encoded. By comparison, classical parity checks are measurements of one logical bit against another, recorded as a third classical bit value. These measurements are performed as required, and the classical bit values are compared over time to detect and correct errors according to the code used. The construction we describe in this paper uses a *coherent* parity check that is similar in spirit to the classical version. Data qubits store the computational information, and their states are compared against each other over time in order to detect errors. In order to keep the stored information undisturbed, the parity check qubits are kept coherent throughout, with the final operations before measurement unentangling them from the data qubits. The classical measurement information is then used to determine any errors.

This is best illustrated by an example. Our first and simplest code is an  $[[11, 3, 3]]$  quantum code, which uses four bit-flip parity check qubits and four phase parity check qubits to protect three data qubits from a single error. The simplest CPC codes are represented graphically using an undirected, *tripartite graph* (we discuss a further, more general, class of codes in the main part of the paper). This  $[[11, 3, 3]]$  code is shown in figure 1.

Nodes represent data, bit-parity, and phase-parity qubits, and edges represent CNOTs between qubits of different types. This type of quantum parity code can thus be defined by three Boolean matrices, specifying the adjacency matrices for each type of permitted edge. In the matrices, a zero represents no edge and a one represents an edge (CNOT).

The  $[[11, 3, 3]]$  code in figure 1 is specified by

$$M^{(B)} = \begin{pmatrix} 1 & 0 & 1 & 0 \\ 1 & 1 & 0 & 0 \\ 0 & 1 & 1 & 0 \end{pmatrix} \quad M^{(P)} = \begin{pmatrix} 1 & 0 & 1 & 0 \\ 1 & 1 & 0 & 0 \\ 0 & 1 & 1 & 0 \end{pmatrix} \quad M^{(C)} = \begin{pmatrix} 0 & 0 & 1 & 1 \\ 1 & 0 & 0 & 1 \\ 0 & 1 & 0 & 1 \\ 1 & 1 & 1 & 1 \end{pmatrix}, \quad (1)$$

where the matrix  $M^{(B)}$  indicates CNOTs between bit flip parity check qubits and data qubits,  $M^{(P)}$  indicates CNOTs between phase parity check qubits and data qubits, and  $M^{(C)}$  indicates CNOTs which serve as cross-checks between the two kinds of parity qubits.

There are many more such codes that can be derived by combining two classical parity codes, one for bit-flips, the other for phase errors. This data, along with a choice of convention for ordering CNOTs, then fixes the encoding and decoding circuits shown in Figure 2. The syndrome measurements shown in that figure then uniquely pinpoint the qubit (data or parity check) where the error occurred, so it can be corrected, if necessary.

Our construction methods for quantum CPC codes enable the machinery of classical parity codes to be imported into quantum error correction, including decode tables. Furthermore, by explicitly tracking all of the possible error propagation, our tools allow us to circumvent the stringent demands of fault tolerance to provide a universal set of encoded quantum gates within one instance of a suitable quantum parity code. These

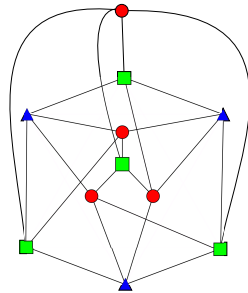


Figure 1: A graphical representation of an  $[[11, 3, 3]]$  CPC code with 3 data qubits (blue triangles), 4 bit-flip parity check qubits (red circles), and 4 phase parity check qubits (green squares). Edges represent CNOT operations between pairs of qubits.

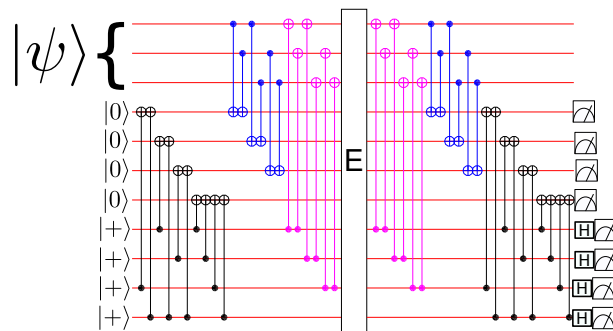


Figure 2: The CNOT operations and measurements for the  $[[11, 3, 3]]$  quantum parity code shown in figure 1 and equation (1). Blue denotes bit-flip checking, magenta phase checking and black cross checking. The boxed ‘E’ indicates a time period in which any single error that occurs can be detected, and hence corrected if required.

can be seen as natural extensions of ancilla-mediated quantum gates (Munro et al., 2005; Anders et al., 2010; Proctor and Kendon, 2016), and build on the use of parity measurements to avoid destroying encoded quantum information introduced by (Munro et al., 2005).

The following sections provide the details to back up these claims. We adopt a pedagogical approach, first introducing codes to correct just bit-flips *or* phase errors in section 2. We provide numerical evidence of their performance for ion trap hardware error parameters in section 2.3. We then develop some tools for constructing codes to handle both bit-flip and phase errors in section 3. We explain first how a simple concatenation does not work, due to error propagation, then provide a solution to detect such propagated errors, if they occur, in section 3.1. We are then ready to describe in section 4 the code introduced above as a fully working quantum parity code. We follow this with numerical results for different error rates, showing how the codes perform in section 4.2. We then show in section 5 that the division into bit-flip and phase errors resulting in two underlying classical codes is not necessary. If parity-check qubits are allowed to check both bit-flip and phase errors, codes based on a single classical parity code can still correct a single error per code block. In section 6 we describe in detail how our codes relate to the stabilizer formalism that most readers will be familiar with.

Having established the basics, we turn to important practical considerations. Codes that can protect qubits continuously, including the encoding and decoding phases of the error correction cycle are covered in section 7. Encoded computation is also a necessity for applications beyond quantum memories. In section 8 we provide methods for encoding gate operations into code cycles, enabling computation to be performed with the same level of protection from errors. We summarise the main implications of our work in section 10.

## 2 Coherent bit-flip correction codes

We begin our presentation of the CPC construction by examining the simplest situation in quantum error correction, with small codes correcting bit-flip errors only (much as one learns about repetition codes by studying the three-qubit repetition code). These codes, which can handle only one bit-flip error, can be understood as *classical* error correction codes with the addition of quantum operations to allow parity information to be stored as quantum rather than classical data. That is, the information is stored coherently, rather than as measured, classical bits.

The fundamental gadget in the CPC construction is the **coherent parity check**. Quantum error correction as it is usually formulated is based on encoding  $n$  logical qubits into  $N$  physical qubits, with  $N - n$  known stabilizer operators. These are measured to produce syndromes, without affecting the logical subspaces into which the logical qubits are encoded. The key to a successful stabilizer code is to be able to tell from a given syndrome, or set of syndromes, where errors have occurred on the physical qubits. This ‘decoding’ is often a difficult problem. Constructing usable stabilizer codes is highly non-trivial. The process of syndrome measurement can be seen as taking a quantum state, encoding it in a larger space, and then measuring quantum data about that state at different times. The resulting classical measurement data from the different times

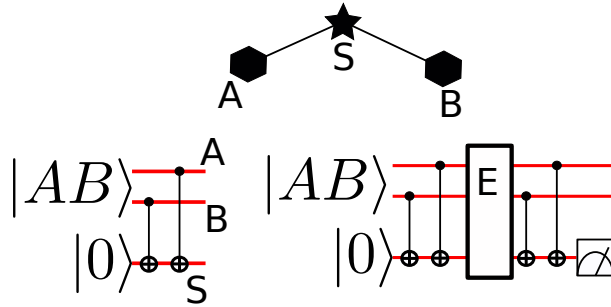


Figure 3: Top: Representation of the bit-flip error detection code as a classical parity check on two bits, with the star representing the check performed by the parity check bit, and the hexagons indicating the bits  $A$  and  $B$  which are having their parity checked. Bottom left: Preparation circuit. Bottom right: two qubit bit-flip error detection circuit, with the stage at which a single, detectable bit-flip error can occur depicted as a box labelled  $E$ .

is compared, to pinpoint errors for subsequent correction. In the most commonly-used construction, based on the repetition-code principle, a single logical qubit is spread across  $N$  physical qubits. Syndrome measurement can be seen as comparing these  $N$  copies with each other. The measurements need to be of stabilizers of this space in order not to disturb the logical information.

We can compare this with the case in classical error processing. A simple classical parity check is a measurement of one logical bit against another, recorded as a third classical bit value (for example, parity bit  $P$  may contain the joint parity of bits  $A$  and  $B$ , with values  $p = a \oplus b$ ). These measurements (non-disturbing, as they are classical), are performed as required, and the classical bit values are compared over time to detect and correct errors according to the code used.

The coherent parity check (CPC) construction presented here starts from the classical notion of parity checking of logical (qu)bits against each other. As we are now in the quantum realm, a direct measurement of one state against another will disturb the states. Rather than expand the space by adding in extra qubits to one with known stabilizers, however, we use a method of performing a parity check coherently. This information is then used to determine any errors. We show that this coherent parity comparison measurement is non-disturbing.

## 2.1 A two qubit coherent parity check

Consider two data qubits  $A$  and  $B$ , which are in the state  $|AB\rangle = \sum_{jk \in \{0,1\}} c_{jk} |jk\rangle$ , an arbitrary superposition expressed in the computational basis  $\{|jk\rangle\}$  for  $j, k \in \{0, 1\}$ . For the purposes of clarity we will initially use pure states. We will use a parity check qubit  $S$ , initialized into the state  $|0\rangle$ , to coherently check whether an error occurs on one of the qubits over a period of time  $t$ . For this simple example, we consider only bit-flip errors, using a simple error model where bit-flip errors occur on individual qubits with probability  $p \ll 1$ , while operations and measurements are perfect.

At the start of the error correction cycle, two CNOTs are performed, the first from  $A$  to  $S$  and the second from  $B$  to  $S$ , as shown in figure 3 (bottom left). The state of  $S$

now contains information about the joint bit-parity of  $A$  and  $B$ . Denoting the encoding CNOTs by  $U_{\text{encode}}$ ,

$$U_{\text{encode}} |AB\rangle |0\rangle = c_{00} |00\rangle |0\rangle + c_{10} |10\rangle |1\rangle + c_{01} |01\rangle |1\rangle + c_{11} |11\rangle |0\rangle, \quad (2)$$

$|S\rangle = |0\rangle$  is associated with even parity, while  $|S\rangle = |1\rangle$  is associated with odd parity.

In the case of a standard syndrome extraction circuit in traditional quantum error correction, qubit  $S$  would now be measured to obtain the result of a  $ZZ$  measurement of  $A$  and  $B$  (where  $Z$  is the Pauli- $Z$  matrix). However, this requires  $A$  and  $B$  to be in an eigenstate of the  $ZZ$  operator, otherwise the measurement will disturb the state. Traditional quantum error correction therefore encodes a single qubit's worth of information into a multipartite state with known stabilizers. In this simple example, the state  $|A\rangle = \alpha |0\rangle + \beta |1\rangle$  would be encoded into the state  $|AB\rangle = \alpha |00\rangle + \beta |11\rangle$ , which is an eigenstate of the  $ZZ$  operator.

By contrast, for a coherent parity check,  $A$  and  $B$  remain raw qubits containing a full two qubit's worth of information. We therefore cannot measure the state of  $S$  after the CNOT operations without disturbing the information. Instead, we keep  $S$  entangled with  $A$  and  $B$ . We now wait for a time  $t$ , during which errors can occur on all three qubits. We assume for the moment that the time for the CNOT operations to be completed is much less than  $t$ . At the end of this time  $t$ , the parity gathering CNOT operations  $U_{\text{encode}}$  are performed again, as in figure 3 (bottom right). In the absence of any errors, the action of the CNOTs is the identity, because they are self-inverse. We therefore recover the separable state  $|AB\rangle |0\rangle$  in the absence of errors. If we now measure  $S$  in the computational basis, we get the result 0, and the state of  $|AB\rangle$  is undisturbed.

This measurement result will change, however, if there is an error on a qubit during the waiting time  $t$ . For example, a bit-flip error occurs on qubit  $A$ , the state at the end of time  $t$  will be

$$X_A U_{\text{encode}} |AB\rangle |0\rangle = c_{00} |10\rangle |0\rangle + c_{10} |00\rangle |1\rangle + c_{01} |11\rangle |1\rangle + c_{11} |01\rangle |0\rangle. \quad (3)$$

The action of the second set of CNOTs leaves the three qubits in the state

$$\begin{aligned} U_{\text{encode}} X_A U_{\text{encode}} |AB\rangle |0\rangle &= c_{00} |10\rangle |1\rangle + c_{10} |00\rangle |1\rangle + c_{01} |11\rangle |1\rangle + c_{11} |01\rangle |1\rangle \\ &= \left( X_A |AB\rangle \right) |1\rangle. \end{aligned} \quad (4)$$

Despite the error, we can see that  $A$  and  $B$  are now disentangled from  $S$ . Moreover, measuring  $S$  now gives the result 1, alerting us to the fact that an error has occurred. Similarly, if the error had occurred on  $B$ , the state just prior to the measurement would be  $(X_B |AB\rangle |1\rangle)$ , and again, a measurement of  $S$  in the computational basis will yield the result 1. We must also consider the case where an error occurred on qubit  $S$  itself,

$$X_S U_{\text{encode}} |AB\rangle |0\rangle = c_{00} |00\rangle |1\rangle + c_{10} |10\rangle |0\rangle + c_{01} |01\rangle |0\rangle + c_{11} |11\rangle |1\rangle. \quad (5)$$

The action of the second set of CNOTs is now

$$\begin{aligned} U_{\text{encode}} X_S U_{\text{encode}} |AB\rangle |0\rangle &= c_{00} |00\rangle |1\rangle + c_{10} |10\rangle |1\rangle + c_{01} |01\rangle |1\rangle + c_{11} |11\rangle |1\rangle \\ &= \left( |AB\rangle \right) |1\rangle. \end{aligned} \quad (6)$$

As before, we have a separable state between  $|AB\rangle$  and  $S$ , and a measurement of the parity check qubit  $S$  yields the result 1 to tell us of the presence of an error.

We can therefore see that in this simple case, coherent parity checking of qubits  $A$  and  $B$  by qubit  $S$  will detect a single error during time  $t$  on any of the three qubits, without destroying the information in  $A$  and  $B$ . If the measurement returns the value 0 we know that no error has occurred (considering only single bit-flip errors), and that the state at the end of the cycle is  $|AB\rangle$ . If the measurement gives the result 1, we know an error has occurred on one of the three qubits, and if we knew which one, we would be able to recover the state  $|AB\rangle$  – the information contained in those qubits has not been irreversibly lost.

While we leave a full density matrix treatment to future work, it is straightforward to see that this fundamental parity check acts identically on impure  $\rho_{AB}$  as pure  $|AB\rangle$ . Consider an impure state of  $AB$ , and purify it using an environment  $E$  (in the case of data in a quantum memory or computer,  $E$  will be other qubits). Then we have a pure state of the full system+environment  $|ABE\rangle$ . If we now run the coherent parity check protocol exactly as above, the encoding step (2) becomes

$$U_{\text{encode}} |ABE\rangle |0\rangle = c_{00} |00E_{00}\rangle |0\rangle + c_{10} |10E_{10}\rangle |1\rangle + c_{01} |01E_{01}\rangle |1\rangle + c_{11} |11E_{11}\rangle |0\rangle \quad (7)$$

where  $E_{ij}$  indexes the state of  $E$  relative to the  $ij$  state of  $AB$ . The parity check qubit  $S$  does not interact with the environment  $E$ , and neither the encode nor decode (either with or without errors) mixes elements of this superposition. The protocol carries through in this extended Hilbert space case exactly as in the case with pure  $|AB\rangle$ . Errors on  $A, B, S$  are flagged with ‘1’, and no error with ‘0’. The protocol acts linearly on each element in the superposition; therefore, even if operations occur on  $E$ , no steering of  $AB$  is possible such that the outcome of the parity check is changed.

The basic gadget of the coherent parity check, then, checks the combined bit-parity of a pair of qubits at two different times in a coherent manner, flagging up if it has changed. This can be viewed as a simple error detection code, able to detect errors on any of the three qubits (data and parity check).

In order to keep continuous checking in operation, this cycle can be repeated as many times as required. If the probability of error is sufficiently small, then the time in between cycles during which the information is unprotected is negligible (a reasonable assumption for many experimental technologies, including the ion trap technology which we will discuss in section 2.3). If measurement and reinitialization of qubit  $S$  is slow (a non-trivial fraction of  $t$ ), then a new parity qubit  $S'$  can be introduced, and a second error detection cycle initiated whilst  $S$  is being measured and reset. Parity checks which cycle through fresh ancilla qubits can continue for as long as is required.

We now use this procedure of coherent parity checking to develop the smallest CPC-constructed code capable of both detecting and correcting single errors.

## 2.2 Three qubit bit-flip error correction

We can accomplish bit-flip error correction using a code with three data qubits and three parity check qubits. We’ll denote this as a  $[[6, 3, 1]]$  code because it can only correct a bit-flip. The classical code that can do this is depicted in figure 4 (top left). Implementation in a coherent quantum circuit is depicted in figure 4 (top right). This code can be

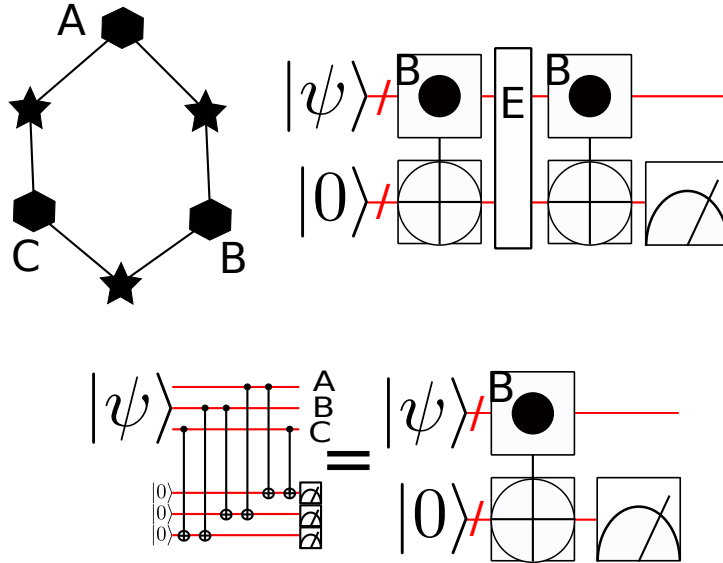


Figure 4: Top left: Classical 3 qubit code capable of correcting single bit errors. Hexagons represent bits, while stars represent parity checks. Top right: Quantum circuit implementation of a classical error correcting code, where  $E$  indicates the stage at which detectable errors might occur. Bottom: Key depicting the meaning of high level symbols used in the top right of this figure as well as various circuit diagrams throughout this paper. The individual CNOTs which compose the circuit in the top right of this figure are given in figure 5.

seen as three overlapping copies of the two-bit error detection code discussed in section 2.1. We also introduce some notation that will be useful for the rest of this paper. The sequence of CNOT operations used for the parity checks is abbreviated as a big, boxed CNOT with **B** indicating these are performing bit-flip parity checks (and **P** indicates phase parity checks). Similarly, the measurements on the parity check qubits are represented by a big measurement symbol. The full circuit for figure 4 is shown in figure 5.

Before discussing the properties of this code, it is useful to put it into the context of standard classical parity codes. In the information theoretical literature, parity codes are often depicted with data bits in one row and parity checks in another row. In this convention the above code takes a more familiar form, Figure 6 (left), in particular when contrasted with the standard  $[7, 4]$  Hamming code, Figure 6 (right). Here  $[N, K]$  denotes that there are  $N$  total bits, and  $K$  data bits, consequently there are  $N - K$  parity checks. In this notation our corresponding classical code is a  $[6, 3]$  code. To later distinguish classical from quantum codes we use the notation  $[[N, K]]$  for a quantum code. Both of these notations are often augmented by a third parameter giving the *code distance*. In the quantum case, this will yield  $[[N, K, 2d + 1]]$ , where  $d$  is the number of correctable (quantum) errors. Since the latter includes both bit and phase error and the above code only corrects for bit errors, it has  $d = 0$  and is thus a  $[[6, 3, 1]]$  code in this notation.

Besides the above graphical representation we can also write our code in terms of the

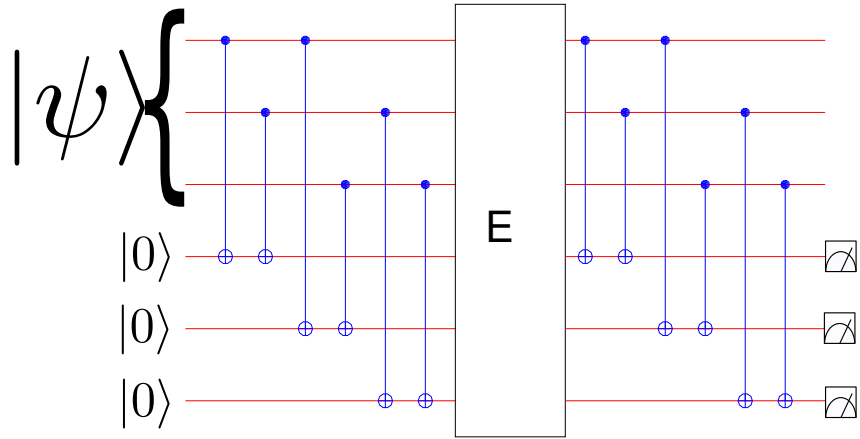


Figure 5: The explicit CNOT operations involved in the circuit shown in figure 4 (top right). Blue denotes bit checking CNOTs.

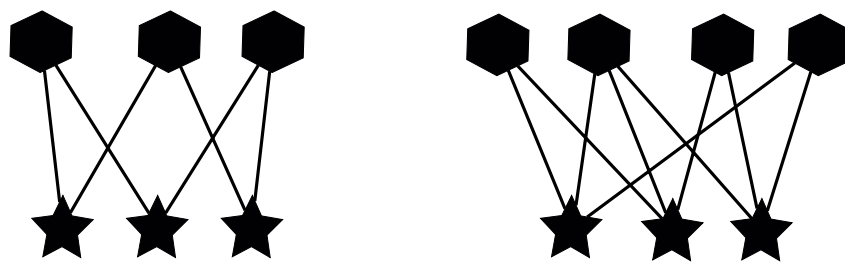


Figure 6: Left: Illustration of the above classical  $[6, 3]$  code in the conventional graphical representation of parity codes. Right: The  $[7, 4]$  Hamming code.

parity matrix,

$$M = \begin{pmatrix} 1 & 0 & 1 \\ 1 & 1 & 0 \\ 0 & 1 & 1 \end{pmatrix}, \quad (8)$$

where rows label data bits and columns parity bits. Here  $M_{ij} = 1$  means that data bit  $i$  participates in parity check  $j$ . The parity matrix  $M$  is closely related to the so-called generator matrix of the code, formally written as,

$$G = [I_K, M], \quad (9)$$

where  $I_K$  is the  $K$ -dimensional identity matrix. The name generator matrix arises from the fact that it generates codes words  $c$  ( $N$ -dimensional vectors) from original data messages  $d$  ( $K$ -dimensional vectors) via the relation  $c = G^T d$ . Both matrices are also closely related to the so-called Hamming matrix

$$H = [M^T, I_{N-K}] \quad (10)$$

which plays an important role in the analysis of classical parity codes, as well as in the construction of larger LDPCs.

We will now show that this classical parity check code is able to correct errors due to single bit-flip errors on any one of the qubits, both data and parity check, during stage  $E$  in figure 4 (top right). We know from the fact that the code depicted in figure 6 is a classical code capable of correcting single errors (showing this is left as an exercise for the reader), that if  $|\psi\rangle$  is a computational basis state, i.e., a classical state, then it will be capable of correcting single bit-flip errors. We therefore need to show it is also capable of protecting  $|\psi\rangle$  from bit-flip errors when it is initialized in an arbitrary quantum state.

It is convenient to use  $E = \cos(\epsilon)\mathbf{1} + i \sin(\epsilon)X$  as our error operator, where  $X$  is the Pauli- $x$  operator. The error operator on all six qubits is thus

$$\begin{aligned} E = & \cos^6(\epsilon)\mathbf{1} + i \sin(\epsilon) \cos^5(\epsilon) \left( \sum_{j \in \{\text{qubits}\}} X_j \right) - \sin^2(\epsilon) \cos^4(\epsilon) \left( \sum_{(j \neq k) \in \{\text{qubits}\}} X_j X_k \right) \\ & - i \sin^3(\epsilon) \cos^3(\epsilon) \left( \sum_{(j \neq k \neq l) \in \{\text{qubits}\}} X_j X_k X_l \right) + \sin^4(\epsilon) \cos^2(\epsilon) \left( \prod_{l \in \{\text{qubits}\}} X_l \sum_{(j \neq k) \in \{\text{qubits}\}} X_j X_k \right) \\ & + i \sin^5(\epsilon) \cos(\epsilon) \left( \prod_{l \in \{\text{qubits}\}} X_l \sum_{j \in \{\text{qubits}\}} X_j \right) - \sin^6(\epsilon) \left( \prod_{l \in \{\text{qubits}\}} X_l \right), \end{aligned}$$

which can be written more compactly as:

$$E = \sum_{n=1}^6 (i^n) \sin^n(\epsilon) \cos^{6-n}(\epsilon) \sum_{\{j_1 \dots j_n\} \in \{\text{qubits}\}} |\epsilon_{j_1 \dots j_n}| \prod_{k \in j_1 \dots j_n} X_k + \cos^6(\epsilon)\mathbf{1}$$

where  $|\epsilon_{j_1 \dots j_n}|$  is the Levi-Civita symbol. For unencoded qubits and  $\epsilon \ll 1$ , it is easily shown that the fidelity of the uncorrected data qubits after a single bit-flip error is  $F_{(\text{no corr})} = |\langle \psi | E | \psi \rangle|^2 \propto 1 - \epsilon^2$ . The fidelity of encoded data qubits is

$$F_{[[6,3,1]]} = \sum_i p_{s_i} |\langle \psi | O_{s_i} | \psi'_{s_i} \rangle|^2,$$

where  $|\psi'_i\rangle$  is the state after implementing the code depicted in figure 4, for parity bit measurements  $s_i$  with  $p_{s_i}$  the probability of measuring  $s_i$ , and  $O_{s_i}$  is an operator which performs relevant corrections based on the syndromes. To demonstrate error correction, we must show that  $F_{[[6,3,1]]} \propto 1 - \epsilon^\eta$  with  $\eta > 2$ .

Starting from an initial state of the data qubits  $|\psi\rangle = \sum_{ijk \in \{0,1\}} c_{ijk} |ijk\rangle$  and the parity qubits in state  $|000\rangle$ , applying the first set of CNOTs to encode the qubits gives the intermediate state

$$\begin{aligned} |\psi_{\text{enc}}\rangle = & (c_{000} |000\rangle + c_{111} |111\rangle) |000\rangle + (c_{001} |001\rangle + c_{110} |110\rangle) |110\rangle \\ & + (c_{010} |010\rangle + c_{101} |101\rangle) |011\rangle + (c_{100} |100\rangle + c_{110} |110\rangle) |101\rangle, \end{aligned} \quad (11)$$

We then apply the error operator followed by the second set of CNOTs measure the parity qubits and apply correction bit-flips as required. We consider each possible set of parity qubit measurement outcomes  $s_i$  in turn. To calculate the fidelity of each of these, we first re-normalize each of the conditional wavefunctions such that  $|\langle \psi'_{ijk} | \psi'_{ijk} \rangle|^2 = 1$  and then calculate the sum of each of these conditional fidelities multiplied by the probability of a the associated syndrome measurement,  $F = \sum_{ijk \in \{0,1\}} p_{ijk} |\langle \psi | \psi'_{ijk} \rangle|^2$ .

**Parity measurements  $s_i = 000$ :** The most likely event leading to this outcome is that no error has occurred, so no corrective bit-flip will be applied. The final state of the data qubits is

$$\begin{aligned} |\psi'_{000}\rangle = & \{ \cos^6(\epsilon) - i \cos^3(\epsilon) \sin^3(\epsilon) (X_A X_B X_C + X_A + X_B + X_C) \\ & + \cos^2(\epsilon) \sin^4(\epsilon) (X_A X_B + X_B X_C + X_A X_C) \} |\psi\rangle \end{aligned} \quad (12)$$

Because no correction has been applied, the fidelity for  $s_i = 000$  is  $|\langle \psi | \psi'_{000} \rangle|^2 = 1 - O(\epsilon^6)$ .

**Parity measurements  $s_i = 001$ :** The most likely events leading to this outcome is that an error has occurred on a parity bit, so no correction is performed, and the final state of the data qubits is

$$\begin{aligned} |\psi'_{001}\rangle = & \{ i \cos^5(\epsilon) \sin(\epsilon) - \cos^4(\epsilon) \sin^2(\epsilon) (X_A + X_C) - i \cos^3(\epsilon) \sin^3(\epsilon) (X_A X_B + X_B X_C) \\ & + \cos^2(\epsilon) \sin^4(\epsilon) X_B + i \cos(\epsilon) \sin^5(\epsilon) X_A X_C \} |\psi\rangle. \end{aligned} \quad (13)$$

The resultant fidelity is  $|\langle \psi | \psi'_{001} \rangle|^2 = 1 - 2\epsilon^2 + \frac{2}{3}\epsilon^4 + O(\epsilon^5)$ . Due to the symmetry of the code,  $|\langle \psi | \psi'_{001} \rangle|^2 = |\langle \psi | \psi'_{010} \rangle|^2 = |\langle \psi | \psi'_{100} \rangle|^2$ .

**Parity measurements  $s_i = 011$ :** The most likely events leading to this outcome is that a single error occurred on data qubit  $C$

$$\begin{aligned} |\psi'_{011}\rangle = & \{ i \cos^5(\epsilon) \sin(\epsilon) X_C - \cos^4(\epsilon) \sin^2(\epsilon) (X_A X_B + \mathbf{1}) - i \cos^3(\epsilon) \sin^3(\epsilon) (X_B + X_A) \\ & + \cos^2(\epsilon) \sin^4(\epsilon) (X_A X_C + X_B X_C) + i \cos(\epsilon) \sin^5(\epsilon) X_A X_B X_C \} |\psi\rangle. \end{aligned} \quad (14)$$

The fidelity is  $|\langle \psi | X_C | \psi'_{011} \rangle|^2 = 1 - 2\epsilon^2 + \frac{2}{3}\epsilon^5 + O(\epsilon^5)$ . By the symmetry of the code,  $|\langle \psi | X_C | \psi'_{011} \rangle|^2 = |\langle \psi | X_B | \psi'_{101} \rangle|^2 = |\langle \psi | X_A | \psi'_{110} \rangle|^2$ .

**Parity measurements  $s_i = 111$ :** In this case the decoding strategy is unclear, as there is no single most likely error. For simplicity, we will assume no correction, whence

$$|\psi'_{111}\rangle = \left\{ i \cos^4(\epsilon) \sin^2(\epsilon) (X_A + X_B + X_C) - i \cos^3(\epsilon) \sin^3(\epsilon) (X_A X_B + X_B X_C + X_A X_C + \mathbf{1}) - \sin^6(\epsilon) X_A X_B X_C \right\} |\psi\rangle. \quad (15)$$

resulting in a code failure, with  $|\langle\psi | \psi'_{111}\rangle|^2 = \frac{\epsilon^2}{3} - \frac{2}{9}\epsilon^4 + O(\epsilon^5)$ . The probabilities of each of the measured results are as follow:

$$\begin{aligned} p_{000} &= 1 - 6\epsilon^2 + 17\epsilon^4 + O(\epsilon^5) \\ p_{001} = p_{010} = p_{100} = p_{011} = p_{101} = p_{110} &= \epsilon^2 - \frac{10}{3}\epsilon^4 + O(\epsilon^5) \\ p_{111} &= 3\epsilon^4 + O(\epsilon^5). \end{aligned} \quad (16)$$

The total fidelity is therefore

$$\begin{aligned} F_{[[6,3,1]]} &= p_{000} |\langle\psi | \psi'_{000}\rangle|^2 + 3p_{001} |\langle\psi | \psi'_{001}\rangle|^2 \\ &\quad + 3p_{011} |\langle\psi | X_C | \psi'_{011}\rangle|^2 + p_{111} |\langle\psi | \psi'_{111}\rangle|^2 = 1 - 15\epsilon^4 + O(\epsilon^5). \end{aligned} \quad (17)$$

The error scales as  $\epsilon^4$  compared with  $\epsilon^2$  for the uncorrected data qubits, hence this code improves the error rate for bit-flip errors on qubits in an arbitrary pure state.

Just as with repetition codes, instead of correcting bit-flips, the same parity check codes can be used to protect the qubits from phase errors. This is accomplished by rotating the basis of all the qubits such that the parity check qubits are now initialized in the  $|+\rangle = \frac{|1\rangle+|0\rangle}{\sqrt{2}}$  state and are the control rather than the target in the CNOTs. Before we discuss codes that can correct both bit-flip and phase errors, it is instructive to characterise the performance of the  $[[6, 3, 1]]$  code numerically for a specific hardware for which it is suitable (fast gates).

## 2.3 Numerical performance of the $[[6, 3, 1]]$ code in ion traps

To numerically model error correction, we must specify some of the device parameters. Motivated by ion trap systems (Harty et al., 2014), we choose a realistic bit-flip error rate<sup>1</sup>, of  $\epsilon_{\text{bit}} = 0.007 s^{-1}$ . Since this code is only able to correct one type of error at a time, for the purposes of illustration we set  $\epsilon_{\text{phase}} = 0 s^{-1}$ . We must also choose an appropriate fidelity metric. This is non-trivial because unlike with codes that protect a single qubit, we should fix a metric that accurately reflects how well we protect multiple qubits simultaneously. We therefore introduce three fidelity metrics.

Firstly, to compare with other codes, we examine the ability of the code to protect single qubits by performing a numerical experiment: We prepare the data qubits all in a bit (phase) eigenstate  $|000\rangle$  ( $|++++\rangle$ ). We then define the fidelity of a single qubit initialized in the appropriate eigenstate to be either

$$F_0 = \sum_{ij \in \{0,1\}} |\langle 0ij | U_{\text{corr}}(\tau) | 000 \rangle|^2, \quad (18)$$

<sup>1</sup>Note that the error rate  $\epsilon$  used in the calculations in section 2 is *not* the same as  $\epsilon_{\text{bit}}$  and  $\epsilon_{\text{phase}}$  in figures 7, 18 and 19. Specifically,  $\epsilon_{\text{bit}}$  and  $\epsilon_{\text{phase}}$  are defined as the probability rate for errors of their respective type, with units of  $s^{-1}$ , while  $\epsilon$  is a unit-less probability amplitude for an error:  $\epsilon \propto \sqrt{\epsilon_{\text{bit}}}$ .

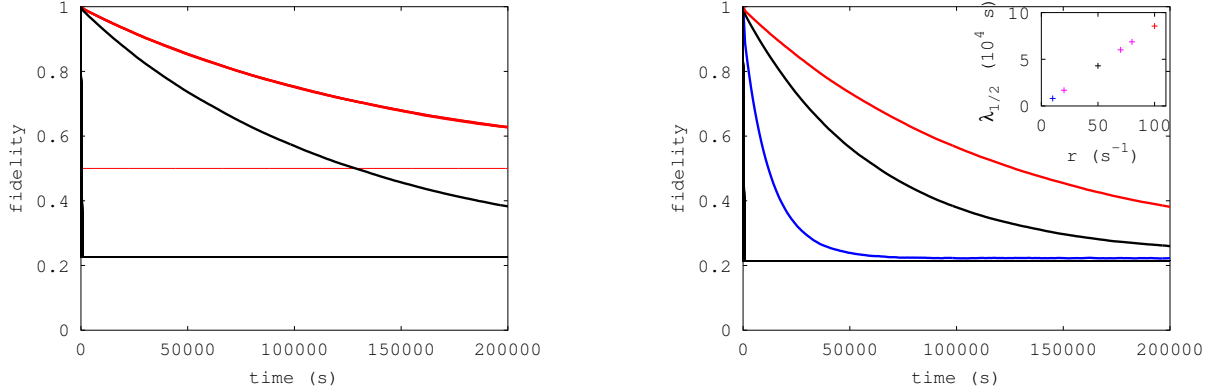


Figure 7: Numerical study of the  $[[6, 3, 1]]$  code (figure 4) using a bit error rate of  $\epsilon_{\text{bit}} = 0.007 \text{ s}^{-1}$  and a phase error rate  $\epsilon_{\text{phase}} = 0 \text{ s}^{-1}$ . Left: Fidelity versus time for a correction cycle rate of  $r = 100 \text{ s}^{-1}$  showing  $F_{\text{rand}}$  (black) from equation (20) and  $F_0$  from equation (18) (red).  $F_+$  from equation (19) remains 1 for all times (not shown). Right:  $F_{\text{rand}}$  for  $r = 10 \text{ s}^{-1}$  (blue),  $r = 50 \text{ s}^{-1}$  (black), and  $r = 100 \text{ s}^{-1}$  (red). Inset: Numerical fit of  $\lambda_{1/2}$  versus cycle rate  $r$  for the three times in the main figure plus others. Thin lines represent curves for unprotected qubits with the same error rate. Error-bars due to statistical fluctuations are smaller than the depicted lines.

or

$$F_+ = \sum_{ij \in \{+, -\}} |\langle +ij | U_{\text{corr}}(\tau) | +++ \rangle|^2, \quad (19)$$

where  $U_{\text{corr}}(\tau)$  is a unitary representing the action of the error correction from time 0 to time  $\tau$ .

Secondly, to characterise the ability to of our code to protect a highly entangled multi-body state, we use the following fidelity metric

$$F_{\text{rand}} = \frac{1}{|R|} \sum_{\psi \in R} |\langle \psi | U_{\text{corr}}(\tau) | \psi \rangle|^2, \quad (20)$$

where we define  $R$  to be a set of randomly generated states drawn from the Haar distribution.

Thirdly, from these two fidelities we define the half life,  $\lambda_{1/2}$  by numerically fitting the data to

$$F_{\text{fit}} = F_{\infty} + (1 - F_{\infty}) \exp\left(-\frac{\log(2)}{\lambda_{1/2}} \tau\right), \quad (21)$$

where  $F_{\infty}$  is a fitting parameter corresponding to the expected value of the fidelity after a long period of time.

In order to run simulations, we also have to choose a correction cycle rate  $r$  appropriate for the system under study. For our error rate of  $\epsilon_{\text{bit}} = 0.007 \text{ s}^{-1}$ , values of  $r$  in the range  $10 \text{ s}^{-1}$  to  $100 \text{ s}^{-1}$  are reasonable. The numerical results are shown in figure 7.

As figure 7 (right) demonstrates, the  $[[6, 3, 1]]$  code (depicted in figure 4) is capable of protecting qubits for a far longer time than the unprotected lifetime of  $\epsilon_{\text{bit}}^{-1} \approx 142 \text{ s}$ , regardless of whether the qubits are entangled with each other. Furthermore, figure 7

(left) shows that state lifetimes scale linearly with  $r$ , indicating that, as the calculations in section 2 show, the protocol is capable of correcting single bit-flip errors on any of the qubits.

## 2.4 Stabilizers and the bit-flip code

We can now start to make contact between the construction of codes based on coherent parity checks, as presented here, and the usual understanding of quantum error correction in terms of stabilizer subspaces and syndrome measurements. General stabiliser codes, which consider the state of one or more qubits to be ‘spread out’ in a non-specific way over a space of codewords (ignoring any qubits that may be used to gather the syndrome information). By contrast, CPC codes make a clear distinction, within this set of codeword states, between which qubits act as data and which act as parity checks. We can see from the 6-qubit code that the CPC construction duplicates *parity comparison* information into the check qubits  $S_1, S_2, S_3$ . This enables a dense storage of information in the code. It also makes sense as the syndromes are interrogated for parity comparison: has eg. the parity of A with respect to B changed? By storing only that information, rather than a copy of the full state, the code is much more efficient. Carrying this parity information forward coherently, in a qubit rather than a classical measurement outcome, allows arbitrary such joint parity measurements to be made, rather than having to measure a stabilizer of the system.

This duplication of parity information into the parity check qubits does, however, give rise to operators across the combined system of data+parity qubits that are then stabilizers of that system. To see how, consider again the action of a single coherent parity check of  $A, B$  by  $S_1$ . The action of the encoding operation is such that, whatever the parity of the joint Pauli operator  $Z_A Z_B$ , this is replicated in the parity of the operator  $Z_{S_1}$ . The three-party system is therefore, after the encoding, in the known  $+1$  eigenstate of the operator  $Z_A Z_B Z_{S_1}$  – irrespective of the states of  $A$  and  $B$ , and without the operator  $Z_A Z_B$  being measured. For the six-qubit code, the stabilizers of the system after the initial encoding are

$$\begin{aligned} Z_A Z_B Z_{S_1} \\ Z_B Z_C Z_{S_2} \\ Z_A Z_C Z_{S_3} \end{aligned} \tag{22}$$

The unencode step can be viewed as measuring these three stabilizer operators. With the straightforward unencode, the second set of CNOTs is a measurement of these operators using the parity check qubits in each (for example,  $Z_A Z_B Z_{S_1}$  is measured using  $Z_{S_1}$ ). In the case of continuous measurement of parity checks, the additional check qubits can be viewed as measuring these three stabilizers, with then an additional SWAP operation between the new and old parity check qubits, so that the old ones are the ones measured. In both cases, though, the final measurement on a parity qubit can be seen in this dual light, as either a temporally extended measurement of a two-party identity operator (comprised of four CNOTs), or as an instantaneous measurement of a three-party stabilizer.

While the identification of stabilizers becomes more complicated as we move to codes

that detect both bit and phase errors, the conclusion carries through: CPC constructed codes are stabilizer codes.

## 2.5 Review of Formalism for Decoding Classical Parity Codes

While the codes in this section are small and can be decoded by a constructed decode table. It is therefore worthwhile to review how the problem of decoding such codes is formulated in a more general context, for codes which are too large to construct an exhaustive decode table. We discuss two equivalent ways in which finding the most likely set of errors (maximum likelihood decoding) can be formulated, firstly as a constrained maximization problem, and secondly as energy minimization with respect to an Ising model.

The probability of each classical bit (represented by a hexagon  $h_i$  in Fig. 6) to be errored is given by  $p_{h_i}$ , and for each parity check (represented by a star  $s_i$ ) the probability to return an incorrect value is  $p_{s_i}$ . The log of the probability that a set of errors has occurred can therefore be written in the following way

$$\log(p_E) = \sum_{i \in \text{hexagons}} \log\left(\frac{p_{h_i}}{1-p_{h_i}}\right) e_{h_i} + \sum_{j \in \text{stars}} \log\left(\frac{p_{s_j}}{1-p_{s_j}}\right) e_{s_j} + C \quad (23)$$

and should be maximized, where  $e \in \{0, 1\}$  is one if a bit or parity check has been errored and zero otherwise and  $C$  is an irrelevant constant shift. This maximization is subject to a set of constraints, however, which are given by the measured results of the parity checks, namely

$$\left( \bigoplus_{j \in \{h\}_{s_i}} e_{h_j} \right) \oplus e_{s_i} = m_{s_i} \forall i \in \text{stars} \quad (24)$$

where  $\{h\}_{s_i}$  indicates the set of hexagons connected by edges to star  $s_i$  and  $m_{s_i} \in \{0, 1\}$  is the parity measurement associated with star  $s_i$  with zero representing an even number of errors and one and odd number and  $\oplus$  indicates a sum modulo 2. A mathematically equivalent representation of this constrained minimization problem is to consider the minimum energy state with respect to the following Ising Hamiltonian acting on a set of spins equal to the number of hexagons where a spin value of 1 represents no error and  $-1$  represents an error and  $Z_{h_i}$  is a Pauli  $Z$  spin matrix acting on spin  $h_i$

$$H_{\text{Ising}} = \sum_{i \in \text{hexagons}} \log\left(\frac{p_{h_i}}{1-p_{h_i}}\right) Z_{h_i} + \sum_{j \in \text{stars}} (-1)^{m_{s_j}} \log\left(\frac{p_{s_j}}{1-p_{s_j}}\right) \prod_{k \in \{h\}_{s_j}} Z_{h_k}. \quad (25)$$

Once it is inferred whether or not each bit was errored from finding the ground state of this Hamiltonian, it can further be deduced that for any parity check which does not match the parity of the number of errors, the parity check itself must have been errored.

The fact that the decode problem for the codes we design within the CPC formalism naturally admits the possibility that an analog Ising model computer (for instance a quantum annealer (*D-Wave Systems Inc. website*, 2016), optical system (Inagaki et al., 2016), or a special purpose CMOS machine (Yamaoka et al., 2016)). In fact the use of a quantum annealer for classical error correction has recently been examined experimentally

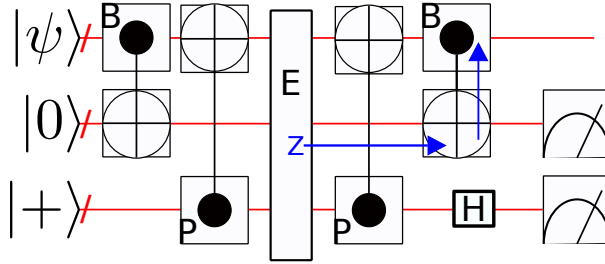


Figure 8: An abstract representation of a code made from concatenating bit and phase parity checks. The arrows illustrate the propagation of undetectable phase error to logical qubits. Key to symbols in figure 4.

(Chancellor, Szoke, Vinci, Aeppli and Warburton, 2016). The techniques in that paper could be extended to a Hamiltonian in the form of Eq. (25) either through specialized hardware (Chancellor, Zohren and Warburton, 2016; Leib et al., 2016) or a variety of mapping techniques (Chancellor, Zohren, Warburton, Benjamin and Roberts, 2016; Bian and et. al., 2014; Rocchetto et al., 2016).

### 3 Tools for constructing full CPC codes

Having shown that coherent parity check codes work for qubits to correct bit and phase errors separately, we now need to build a code which can correct both bit-flip and phase errors at the same time. We continue the pedagogical approach by first illustrating why the naive approaches don't work, then introducing the tools we need to fix the problems and hence create a working code.

Taking three data qubits as before, the most naive way to go about correcting both bit-flip and phase errors is to use, not one, but two sets of parity check qubits. One set is initialized in  $|000\rangle$  for bit-flips, the other is initialized in  $|+++ \rangle$  for phase errors. We then perform CNOTs with the bit-flip parity check qubits, followed by CNOTs with the phase parity check qubits. After some time, during which errors may occur, we check for errors by just reversing the order of the CNOTs, first phase then bit-flip. This is shown schematically in figure 8.

If the bit-flip and phase checks are based on a well-designed classical code, such as the three bit code used in section 2.2, or the Hamming (7, 4) code, then the simple construction given in the previous paragraph will yield unique signatures for all errors on the set of data qubits which are being checked. Moreover, it can correct and detect bit-flip errors on the qubits which check for bit-flip errors, and phase errors on the qubits which check for phase errors. However, there is a fatal flaw in this construction: bit-flip errors on the parity check qubits for phase errors will be propagated back to the logical qubits in a completely undetected way, as shown by the arrow on figure 8. Although phase errors on the qubits which check for bit-flip errors will also be propagated, this will happen before the CNOTs which check for phase errors, and therefore should be detected and corrected in a well-designed code.

Given the undetected error propagation in the naive approach, we clearly need to add extra checks to cover all the possible errors on all the qubits. If we add more CNOTs so

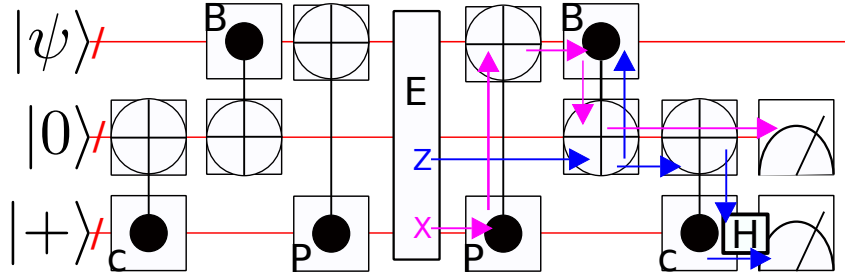


Figure 9: An abstract representation of the quantum circuit to build a code by concatenating bit-flip and phase parity checks with additional ‘cross check’ CNOTs between bit-flip and phase parity check qubits. Blue arrows show that the same kind of phase error arrow which was undetectable in figure 8 is now detectable and therefore correctable. Magenta arrows show the propagation for the bit-flip errors on the phase parity check qubits. Key to symbols in figure 4.

that bit-flip and phase parity check qubits check each other for errors as well as checking the data qubits, we arrive at the code illustrated in figure 9. The addition of more CNOTs with phase parity check qubits acting as controls, and bit-flip parity check qubits acting as targets attempts to catch the errors that went undetected in the code in figure 8. These CNOTs track bit-flip errors on phase parity check qubits, and phase errors on bit-flip parity check qubits, which can now show up in the measurement of the opposite type of parity qubit. Unfortunately, this is not yet a fully functional qubit parity code. To see why this still fails, we need some more tools to analyse the functioning of the code.

### 3.1 Graphical tools for parity codes

From the way in which the quantum circuits for parity codes are constructed, as illustrated in figure 9, we can represent these codes as a tripartite graph in which three types of nodes represent data qubits, bit-flip parity check qubits, and phase error parity check qubits. Because bit-flip parity check qubits will always be targets of CNOTs, and phase error parity check qubits will always be controls, the direction of a CNOT is defined by the structure of the code. Hence, an undirected tripartite graph is sufficient to represent a parity code.

Figure 10 shows an  $[[11, 3, 1]]$  code which extends the  $[[9, 3, 1]]$  code from figure 9 with two additional qubits. These extra qubits check the bit-flip and phase parity check qubits for phase and bit-flip errors respectively, to identify the propagating errors. Figure 11 illustrates the rules to translate between this tripartite graph representation and a quantum circuit representation.

The undirected graph of figure 10 can also be mathematically represented as an adjacency matrix. Moreover, the tripartite structure of the graph imposes additional constraints on this matrix, namely, that the only non-zero matrix elements can be between nodes of different types. Thus, a quantum parity code can be defined by three Boolean matrices in which a zero represents no edge and a one represents an edge. We call the matrix representing edges (CNOTs) between bit-flip check parity qubits and data qubits  $M^{(B)}$ , the one representing edges between phase flip check parity qubits  $M^{(P)}$ , and the one representing edge between the two types of parity checking qubits  $M^{(C)}$ . For the

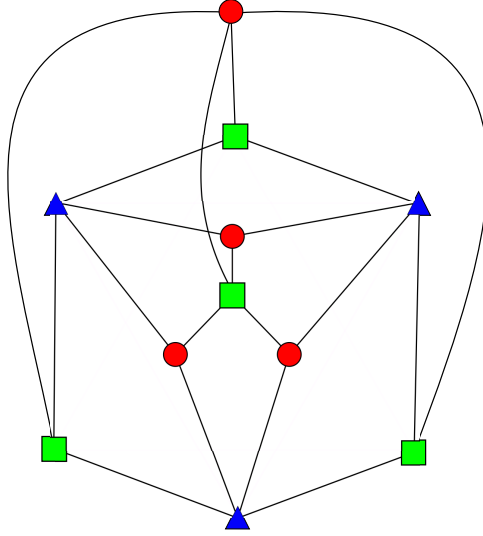


Figure 10: An  $[[11, 3, 1]]$  code represented as a tripartite graph. Triangles represent data qubits, circles represent bit-flip parity check qubits and squares represent phase parity check qubits. Rules for translating this graph into a quantum circuit are given in figure 11. The adjacency matrix for this graph is defined in equation (26).

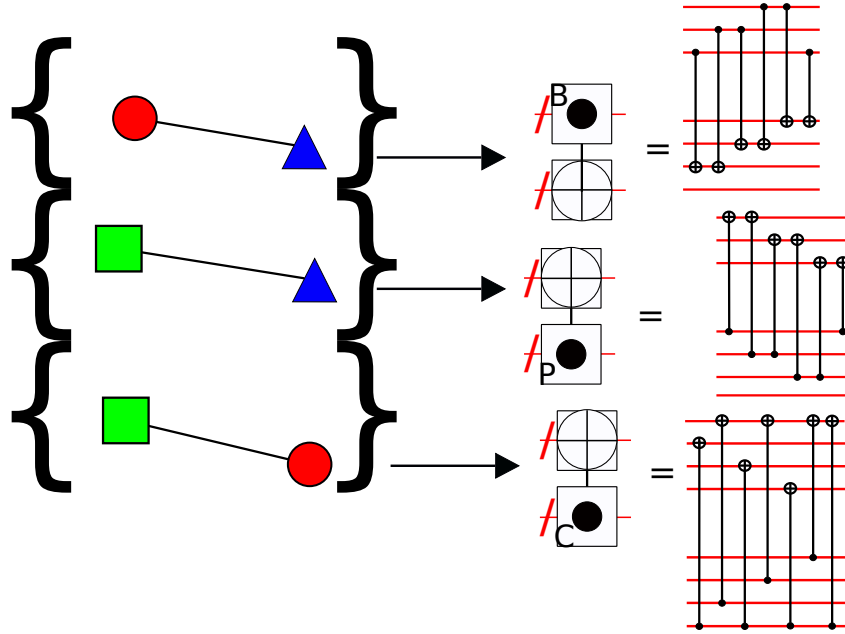


Figure 11: Diagrammatic representation of the translation from a tripartite graph to a parity code for the code illustrated in figure 10.

code depicted in figure 10, these matrices are,

$$M^{(B)} = \begin{pmatrix} 1 & 0 & 1 & 0 \\ 1 & 1 & 0 & 0 \\ 0 & 1 & 1 & 0 \end{pmatrix} \quad M^{(P)} = \begin{pmatrix} 1 & 0 & 1 & 0 \\ 1 & 1 & 0 & 0 \\ 0 & 1 & 1 & 0 \end{pmatrix} \quad M^{(C)} = \begin{pmatrix} 0 & 0 & 0 & 1 \\ 0 & 0 & 0 & 1 \\ 0 & 0 & 0 & 1 \\ 1 & 1 & 1 & 1 \end{pmatrix}, \quad (26)$$

where the vertical index of the first two matrices represents data qubits, with the horizontal representing parity check bits and for the third matrix the vertical index represents bit-flip check parity qubits and the horizontal represents phase check parity qubits. To be explicit, the full adjacency matrix in terms of these three matrices is

$$M^{\text{Full}} = \left( \begin{array}{c|c|c} - & M^B & M^P \\ \hline (M^B)^T & - & M^C \\ \hline (M^P)^T & (M^C)^T & - \end{array} \right) \quad (27)$$

where the three blocks of the matrix (horizontally left to right and vertically top to bottom) comprise data, bit, and phase qubits respectively.

We will see, however, that the code in equation (26) is still *not* able to correct arbitrary single qubit errors, and is included for pedagogical reasons - fully working examples are presented in section 4. There are some further considerations that will assist us in understanding this and other quantum parity codes.

**Canonical Ordering:** The choice to perform the CNOTs between the data qubits and the bit-flip check parity qubits before the phase check CNOTs seems somewhat arbitrary. However, the commutators between CNOTs which connect the data qubits to bit-flip check parity qubits and those which connect them to phase check parity qubits are themselves CNOTs between the two types of parity check qubits, a circuit transformation can always be found which represents the code in the form illustrated in figure 9. We will now show that ordering in this way allows us to represent the propagation of errors in this code with simple graphical rules.

**Rules for Error Propagation:** While the edges we have drawn in figure 10 do uniquely define a parity code, they do not tell the entire story of error propagation within the codes. Bit-flip errors will travel from control to target on the CNOTs, and phase errors from target to control. Because the bit-flip error parity check qubits are always targets, and the phase error check parity qubits are always controls, the edges do show pathways for the relevant errors to travel in terms of detection, but there is one pathway for errors to be detected which is not depicted in this type of figure. This path is taken by bit-flip errors on the phase parity check qubits and is illustrated by the magenta arrows in figure 9.

Fortunately, the propagation of these errors can be understood as simple graphical rules. This propagation can be represented graphically by arrows (directed edges) from squares (phase parity check qubits) to circles (bit-flip parity check qubits) which are both connected to the same triangle (data qubit) by edges. If an edge already exists between this square and circle, the error propagated directly through this CNOT will cancel with the one propagated indirectly through the data bit, and therefore an arrow should be drawn going from the circle to the square rather than the square to the circle. If a circle, square pair are connected through two triangles, then the propagated error will cancel, returning to the original graph. This rule continues such that an arrow should be drawn between pairs connected by an odd number of triangles, but not for those connected by an even number. See figure 12 for an illustration of these rules pictorially. Applying these rules to the code depicted in figure 10 results in the propagation depicted in figure 13.

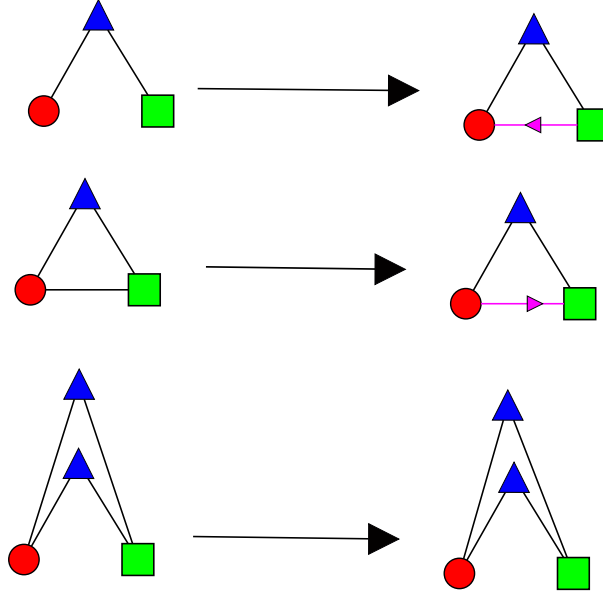


Figure 12: Pictorial representation of error propagation rules under canonical ordering of syndrome gathering. Top: arrow is drawn from square (phase check parity qubit) to circle (bit-flip check parity qubit) if they are mutually connected to an even number of triangles (data qubits). Mid: If an edge already exists between them reverse the direction of the arrow. Bottom: Do nothing for pairs mutually connected to an even number of triangles.

### 3.2 Effective classical parity codes

We can now define *effective* classical parity codes from which fully functional quantum parity codes can be constructed. We will do this by example. Equipped with the pictorial representation for how errors propagate, two effective classical codes, one for bit-flip errors, and one for phase errors can be extracted. For each of these types of errors, the parity check qubits corresponding to that kind of error will act as effective parity checks, with all undirected edges, plus directed edges which are directed toward the relevant checks, determining which qubits are checked for errors. The protocol for drawing the effective bit-flip (phase) error classical code is as follows:

*All circles (squares) become parity checks, while all other nodes become the bits which are being checked. Each parity check is performed between all other nodes connect to a circle (square) either by undirected edges, or arrows which are directed toward the circle (square). Undirected edges between squares and triangles (circles and triangles) have no effect on this effective code, as do directed edges which are directed toward squares (circles).*

By following this protocol twice, once for bit-flips (circles) and once for phase errors (squares), the  $[[11, 3, 1]]$  quantum parity code defined in figure 10 leads to the two effective classical codes in figure 14. Demonstrating the utility of our graphical methods, we can see that the quantum parity code depicted in figure 10 allows undetectable single qubit phase errors which can be propagated to the data bits.

It is worth pointing out at this point that not every error on parity check bits needs to be corrected. Errors propagate to the data qubits via CNOTs with the parity check

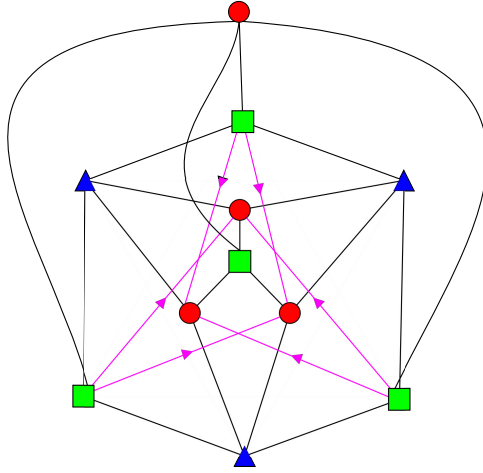


Figure 13: An extension of figure 10 which also includes error propagation by the graphical rules depicted in figure 12

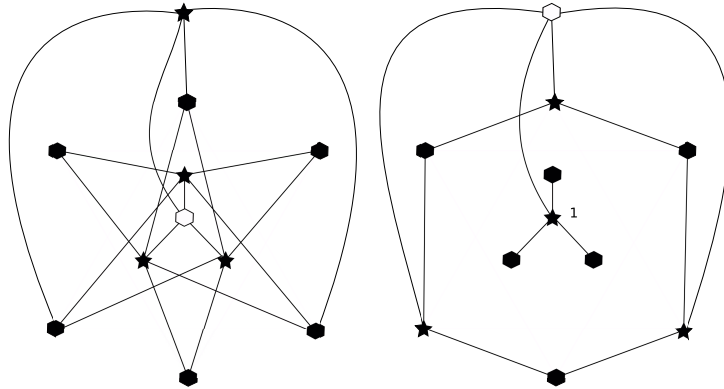


Figure 14: Effective classical codes for bit-flip errors (left) and phase errors (right) for the  $[[11, 3, 1]]$  quantum parity code depicted in figure 10. Hexagons represent effective bits being checked for errors, and stars represent parity checks. Unfilled hexagons indicate parity check qubits which do not share any CNOTs with data qubits and therefore do not need to be corrected because they cannot propagate errors to the data. While the left code is a good classical code in the sense that any single bit error gives a unique signature in terms of parity checks (and therefore can be corrected), the right code is not, an error on any of the three bits which are checked by the parity check labeled 1 (or on the check bit itself) will give the same signature.

qubits which check them. Therefore, parity check qubits which *only* check other parity check qubits will not be able to propagate errors to the data qubits, and errors on these qubits do not need to be corrected.

### 3.3 Proof of Graphical Formalism for Propagation

It is straightforward to prove that the graphical formalism in the previous section is correct. To do this, we first appeal to causality, any operation performed after the CNOTs which act on a given set of qubits, such as the bit-flip or phase check qubits will have

no effect on the measured state of these qubits. Therefore, if we transform the decoder circuit into one for which these operations are performed first, then these CNOTs will define the propagation of information to these qubits and all later operations can be ignored. Explicitly, if we define  $\text{CNOT}(i, j)$  as a CNOT with control qubit  $i$  and target  $j$ , in mathematical terms we want to convert the decoder circuit to one of the form <sup>2</sup>

$$U_{\text{decode}} = \prod_p^{|C^b|} \text{CNOT}(C_p^b, T_p^b) \prod_q^{|C^a|} \text{CNOT}(C_q^a, T_q^a), \quad (28)$$

where we assume this unitary acts to the right,  $|\phi'\rangle = U_{\text{decode}} |\phi\rangle$ . To determine the propagation of phase information we require that  $C_q^a \in P$ ,  $T_q^a \notin P \forall q$  and  $C_q^b \notin P \forall p$  where  $P$  is the set of phase parity check qubits. Once in this form, the phase parity information collected by each of the parity check qubits is just described by the set of target qubits  $\{T^a\}$ . Similarly, to determine the propagation of bit-flip information, we should perform a circuit transformation such that  $T_q^a \in B$ ,  $C_q^a \notin B \forall q$  and  $T_q^b \notin B \forall p$ . In this case, the bit-flip parity information on each qubit is determined by the set of controls  $\{C^a\}$ .

To perform the necessary transformations, we must consider the commutation rules for CNOT matrices

$$\begin{aligned} [\text{CNOT}(i, j), \text{CNOT}(k, l)] = & \text{CNOT}(i, l) \delta_{j,k} (1 - \delta_{i,l}) + \text{CNOT}(k, j) \delta_{i,l} (1 - \delta_{j,k}) \\ & + \delta_{j,k} \delta_{i,l} U'(i, j), \end{aligned} \quad (29)$$

where  $\delta$  is the Kronecker delta, and  $U'(i, j)$  is a unitary operation the exact form of which is not required for this discussion. From this commutation relation, we immediately see that the cross check CNOTs commute with both the bit-flip and phase checking CNOTs, meaning that all CNOTs can be moved to the beginning of the circuit trivially. The parity checks for phase errors are therefore defined only by the graph CNOTs for which these qubits are the controls. The graphical propagation rules given in the previous section clearly never change this structure, and therefore are equivalent to a classical code with the measurements on the phase check qubits acting as parity measurements, and the bits which are measured defined by the relevant CNOTs.

On the other hand, the bit-flip check CNOTs and the phase checking CNOTs do *not* in general mutually commute. Therefore, to change the order of CNOTs such that these are performed first, we must insert the commutator between these two sets of CNOTs. By the rules given in equation (29), the commutator itself will have phase parity check qubits as the controls and bit-flip parity check qubits as the targets, so will itself commute with the other sets of CNOTs. Equation (29) indicates that for a bit-flip and phase parity check acting on the same data qubit, the commutator will form an additional CNOT with the phase parity check qubit as control and the bit-flip parity check qubit as the target. This is equivalent to the graphical rule depicted on the top of figure 12.

To derive the other two graphical rules, we appeal to another property of the CNOT, it is self inverse, i.e.,  $\text{CNOT}(i, j) \text{CNOT}(i, j) = \mathbf{1}$ . This means that if a CNOT is already present between the two relevant qubits, either due to a previous commutation or to a

---

<sup>2</sup>Note that in general these CNOTs will not commute, so the products in this expression are ordered, i.e.  $\prod_{j=1}^3 A_j = A_3 A_2 A_1$  which is not necessarily equal to  $A_1 A_2 A_3$ .

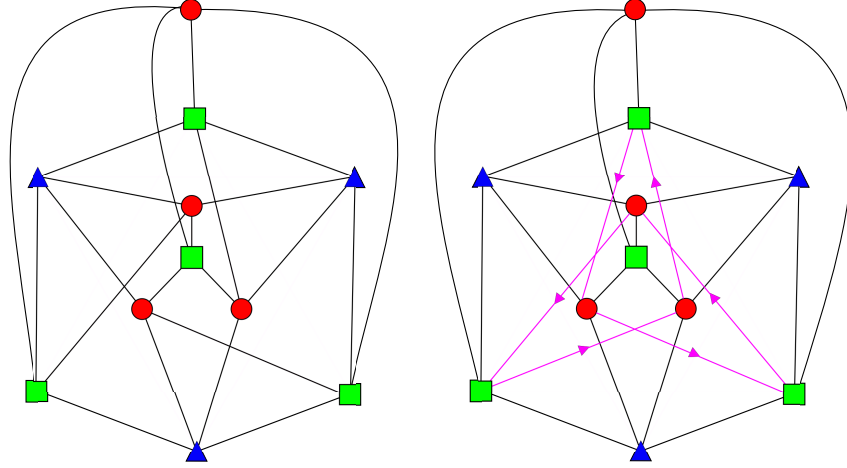


Figure 15: Left: Graphical representation of an  $[[11, 3, 3]]$  code with 3 data qubits (triangles), 4 bit-flip parity check qubits (circles), and 4 phase parity check qubits (squares). The adjacency matrix for this graph is defined in equation (30). Right: Same, but also including error propagation calculated by the graphical rules in figure 12.

cross check, then that CNOT will be canceled out by the commutation. If the CNOT is from a cross check, this will lead to the middle rule in figure 12, where the cross check is still able to act on the phase information, but not on the bit-flip information. On the other hand, if the CNOT is due to a previous commutation, the error propagation cancels completely as depicted on the bottom of figure 12.

## 4 Full CPC codes to correct single errors

Equipped with the set of tools developed in the previous section, we are finally ready to construct fully-functional quantum parity codes. We now present two examples of fully working small quantum parity codes.

### 4.1 Two small quantum parity codes

The  $[[11, 3, 1]]$  code depicted in figure 10 and defined by the matrices in equation (26) almost works. By adding some extra cross check CNOTs, we can create an  $[[11, 3, 3]]$  code which appears in figure 15. The matrices defining this new code are,

$$M^{(B)} = \begin{pmatrix} 1 & 0 & 1 & 0 \\ 1 & 1 & 0 & 0 \\ 0 & 1 & 1 & 0 \end{pmatrix} \quad M^{(P)} = \begin{pmatrix} 1 & 0 & 1 & 0 \\ 1 & 1 & 0 & 0 \\ 0 & 1 & 1 & 0 \end{pmatrix} \quad M^{(C)} = \begin{pmatrix} 0 & 0 & 1 & 1 \\ 1 & 0 & 0 & 1 \\ 0 & 1 & 0 & 1 \\ 1 & 1 & 1 & 1 \end{pmatrix}. \quad (30)$$

and the explicit circuit is in figure 16.

To show that this code works without undetected error propagation, we obtain the two effective classical codes, which are depicted in figure 17. Upon inspecting these codes, we find that both classical codes provide unique signatures for single bit errors. Hence, this

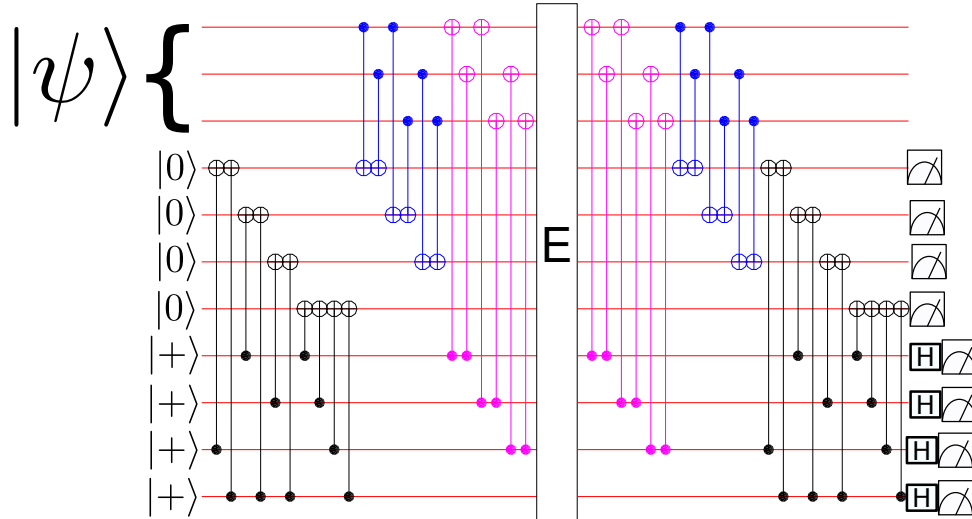


Figure 16: Explicit CNOTs involved in the code in equation (30) and illustrated in figure 15 (left). Blue denotes bit-flip checking CNOTs, magenta phase checking and black cross checking.

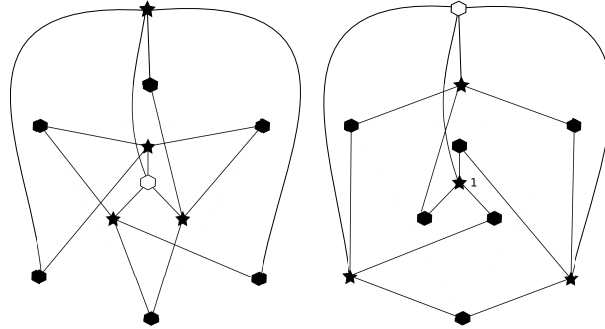


Figure 17: Effective classical codes for bit-flip errors (left) and phase errors (right) for the  $[[11, 3, 3]]$  parity code depicted in figure 15. Hexagons represent effective bits being checked for errors, and stars represent parity checks. Unfilled hexagons indicate parity check qubits which do not share any CNOTs with data qubits and therefore do not need to be corrected because they cannot propagate errors to the data. Both codes provide unique parity check signatures for all single qubit errors, including the two errors which need not be corrected.

$[[11, 3, 3]]$  quantum parity code is capable of correcting arbitrary single qubit errors. This is just one of many quantum parity codes. For example, we have also found a  $[[12, 4, 3]]$  quantum parity code, based on the Hamming (7, 4) code, which can protect four data qubits from arbitrary single qubit errors, while still having only four bit-flip parity check qubits and four phase parity check qubits. The adjacency matrices for this code are:

$$M^{(B)} = \begin{pmatrix} 1 & 0 & 1 & 0 \\ 1 & 1 & 0 & 0 \\ 1 & 1 & 1 & 0 \\ 0 & 1 & 1 & 0 \end{pmatrix} \quad M^{(P)} = \begin{pmatrix} 1 & 0 & 1 & 0 \\ 1 & 1 & 0 & 0 \\ 1 & 1 & 1 & 0 \\ 0 & 1 & 1 & 0 \end{pmatrix} \quad M^{(C)} = \begin{pmatrix} 0 & 0 & 1 & 1 \\ 1 & 0 & 0 & 1 \\ 0 & 1 & 0 & 1 \\ 1 & 1 & 1 & 1 \end{pmatrix}. \quad (31)$$

It is not instructive to demonstrate that this code also works, because this is a mechanical

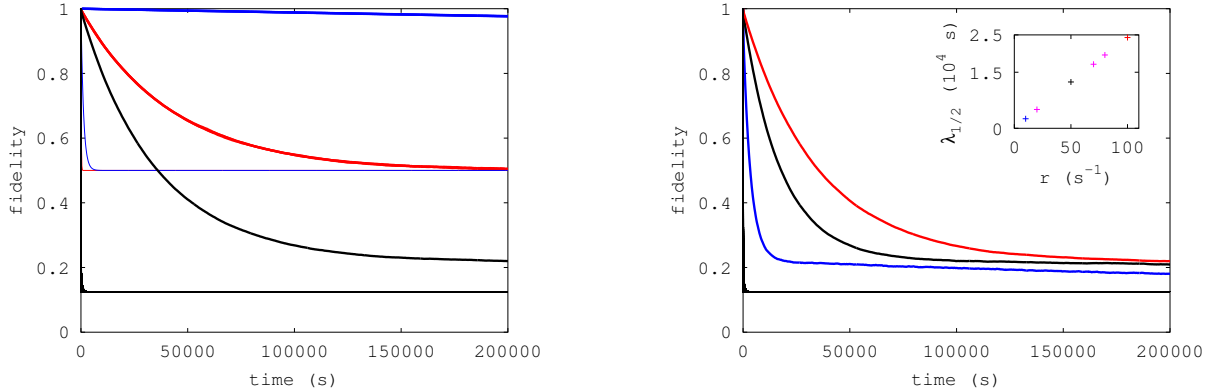


Figure 18: Numerical results for the  $[[11, 3, 3]]$  quantum parity code in figure 15 and equation (30) using a bit-flip error rate of  $\epsilon_{\text{bit}} = 0.007 \text{ s}^{-1}$  and a phase error rate  $\epsilon_{\text{phase}} = 0.0007 \text{ s}^{-1}$ . Right: Fidelity versus time for a correction cycle rate of  $r = 100 \text{ s}^{-1}$ . The black curve depicts  $F_{\text{rand}}$  from equation (20). The overlapping red curves depicts  $F_0$  defined in equation (18). The overlapping blue curves depicts  $F_+$  defined in equation (19) for each individual qubit. Left:  $F_{\text{rand}}$  for  $r = 10 \text{ s}^{-1}$  (blue),  $r = 50 \text{ s}^{-1}$  (black), and  $r = 100 \text{ s}^{-1}$  (black). Inset: Numerical fit of  $\lambda_{1/2}$  versus cycle rate  $r$  for the three times in the main figure plus others. Thin lines represent curves for unprotected qubits with the same error rate. Error-bars due to statistical fluctuations are smaller than the depicted lines.

procedure which follows the same steps we have shown for two other codes. It is therefore left as “an exercise for the reader”.

## 4.2 Numerical tests of $[[11, 3, 3]]$ and $[[12, 4, 3]]$ codes

Now that we have two working quantum parity codes, we test these codes numerically, as we did in section 2.3 for the single error  $[[6, 3, 1]]$  code. Because we want to demonstrate that these codes can correct both bit-flip and phase errors, we now choose bit-flip and phase error rates relevant for the NQIT ion trap system (see (Harty et al., 2014) and related work),  $\epsilon_{\text{bit}} = 0.007 \text{ s}^{-1}$  and  $\epsilon_{\text{phase}} = 0.0007 \text{ s}^{-1}$ . Figure 18 presents numerical results for the  $[[11, 3, 3]]$  code given in equation (30). The lifetimes are able to be extended well beyond the limitation of the unprotected lifetime of a single qubit due to bit-flip errors ( $\frac{1}{\epsilon_{\text{bit}}} \approx 142 \text{ s}$ ) and even well beyond those due to the less probable phase errors ( $\frac{1}{\epsilon_{\text{phase}}} \approx 1,420 \text{ s}$ ). Moreover, the lifetime scales linearly with  $r$ , confirming that the codes are able to correct arbitrary single qubit errors.

In figure 19, we show numerical results for the  $[[12, 4, 3]]$  quantum parity code defined in equation (31). As for the  $[[11, 3, 3]]$  code, these plots confirm that the  $[[12, 4, 3]]$  code does correct single qubit errors. It is also worth noting that, unlike the two other codes which we have examined numerically, the  $[[12, 4, 3]]$  code does not have a symmetry between the data qubits, as a result, one of the qubits is slightly more susceptible to errors than the other three. This is because detectable errors of a given type can be propagated to the third data qubit from three of the parity check qubits, while for the other three data qubits, only two parity check qubits propagate errors.

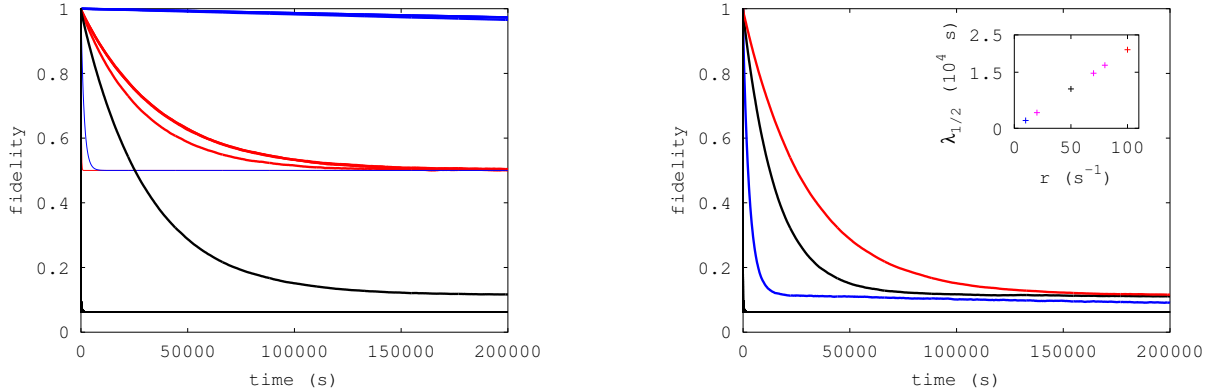


Figure 19: Numerical results for the  $[[12, 4, 3]]$  quantum parity code defined in equation (31) using a bit error rate of  $\epsilon_{\text{bit}} = 0.007 \text{ s}^{-1}$  and a phase error rate  $\epsilon_{\text{phase}} = 0.0007 \text{ s}^{-1}$ . Right: Fidelity versus time for a correction cycle rate of  $r = 100 \text{ s}^{-1}$ . The black curve depicts  $F_{\text{rand}}$  from equation (20). The overlapping red curves depicts  $F_0$  defined in equation (18), but for four data qubits. The overlapping blue curves depict a four qubit version of  $F_+$  defined in equation (19) for each individual qubit. Left: A four qubit version of  $F_{\text{rand}}$  for  $r = 10 \text{ s}^{-1}$  (blue),  $r = 50 \text{ s}^{-1}$  (black), and  $r = 100 \text{ s}^{-1}$  (black). Inset: Numerical fit of  $\lambda_{1/2}$  versus cycle rate  $r$  for the three times in the main figure plus others. Thin lines represent curves for unprotected qubits with the same error rate. Error-bars due to statistical fluctuations are smaller than the depicted lines.

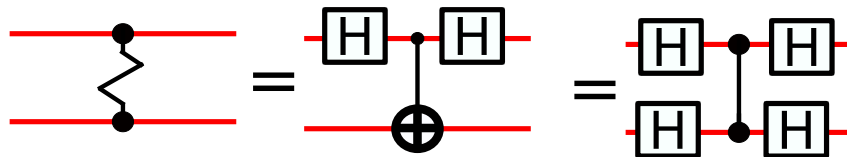


Figure 20: Gate for translating phase error parity information to bit-flip parity information. This gate is the conjugate of the controlled-Z gate.

## 5 Combining bit-flip and phase checks

The methods we have discussed so far are for constructing codes which search for changes in bit-flip and phase parity independently. However, there is no fundamental reason why this has to be done separately. Phase error information can be collected onto the bit-flip parity check qubits by rotating to the conjugate basis on the control before performing a CNOT, and then rotating back. As figure 20 illustrates, this gate is the controlled-Z acting in the conjugate basis.

In principle, we could use a normal controlled-Z to collect bit-flip information onto phase error parity check qubits. However, when parity check qubits can contain both types of information, the difference between bit-flip and phase parity check qubits is no longer meaningful. All the parity check qubits can thus be initialized in the  $|0\rangle$  state and measured in the computational basis. Furthermore, cross checks, where two qubits each check the phase error information of the other, can be performed between any pair of these parity check qubits. This leads to a total circuit structure of the form depicted in figure 21.



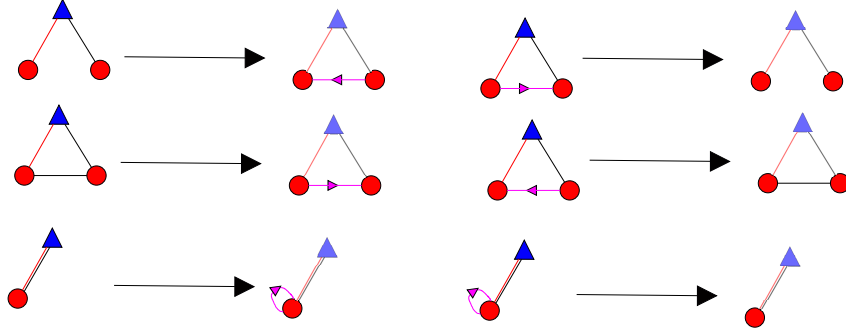


Figure 22: Rules for error propagation in general quantum parity codes. Faded colour indicates that each connection through a triangle should be considered exactly once.

circle through a triangle by a black edge followed by a red edge, this arrow will start at the circle which connects to the black edge and be directed toward the circle which connects to the red edge. If a black edge already exists between these two nodes, then the direction of the arrow is reversed.

When creating these arrows, we should consider every pair of circles connected by a single triangle through both red and black edges exactly once. If an arrow going in the same direction already exists between the pair of nodes, then the arrow will be removed, but if one in the opposite direction exists, the arrow becomes a black edge. A net result of this process is to add an arrow in a given direction *iff* an odd number of connections through triangles in that direction exist (in terms of red and black nodes). If a circle is connected to the same triangle by both a red and black edge, then the propagation will generate a *self loop* on the circle, an even number of self loops cancel, while an odd number of self loops are equivalent to a single self loop. Note that no propagation occurs if the connection is through either a pair of red edges or a pair of black edges. The graphical rules for these more general codes are summarized in figure 22.

**From Graphical Representation To Classical Code:** Now that we have established the propagation of information graphically, we need to translate this representation into a classical code. To do this, we have to represent the phase and bit information of each parity check qubit and data qubit separately. Because our measurements measure the bit information of the parity check qubits, these turn into the checks (represented by stars), while the phase information of each of these becomes a classical bit to be checked (represented by hexagons). Neither the bit nor the phase information of the data qubits is measured, so each of these becomes two hexagons. The edges which represent which bits are checked by each parity check are determined by the edges of the graph. The procedure to produce the graph of the classical code is as follows:

*First turn all triangles into a pair of bits (hexagons), one to the left and one to the right. Each circle becomes a bit (hexagon) and a check (star). A black (red) edge between a circle and a triangle becomes a check acting on the right (left) bit resulting from the triangle. A black edge between two circles becomes a check between each circles' bit and the check created from the other circle. An arrow between two circles means that the check from the origin of the arrow checks the bit from the target of the arrow. A self loop means that the check resulting from a circle checks the bit associated with the same circle.*

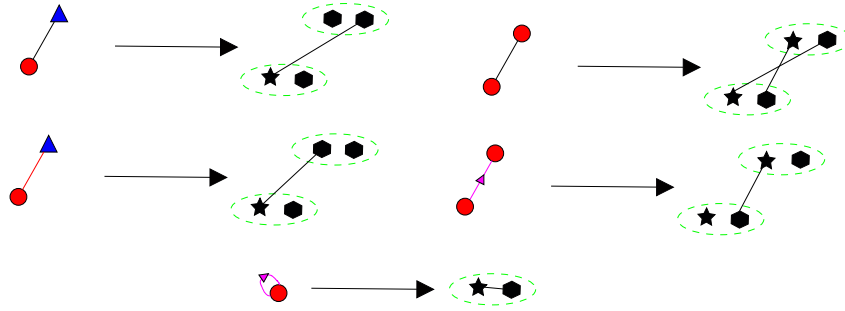


Figure 23: Rules for creating classical codes in the more general formalism after error propagation has been calculated. Dashed green circles represent pairs of bits or bits and checks created from the same qubit.

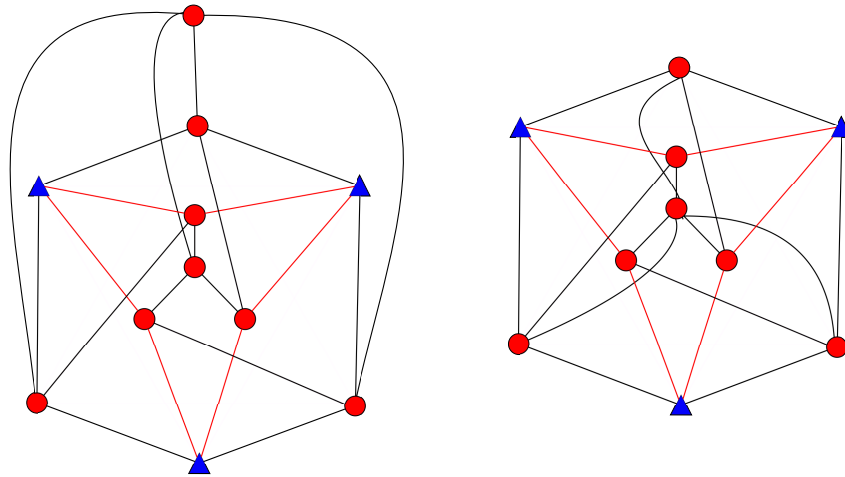


Figure 24: Left: The code in figure 1 in the more general graphical representation. Right: Modifying this code by performing the check for all phase errors on the parity check qubits with a single qubit rather than one for each.

Any combinations not listed cannot be produced from the propagation rules given previously. The procedure is illustrated graphically in figure 23.

## 5.2 Turning the $[[11, 3, 3]]$ code into $[[10, 3, 3]]$

Let us consider a simple example of what this more general construction for quantum parity codes can accomplish. Take the  $[[11, 3, 3]]$  code in figure 1 and represent it in the more general graphical format, as depicted in figure 24 (left). This is done by first making all edges between circles and triangles red, and then turning all squares to circles. We can now modify the code so that all checks for phase errors on the parity check qubits are performed by a single qubit, thereby reducing the total number of qubits by one, and creating a new  $[[10, 3, 3]]$  code. With this modification, the code can no longer be represented by the methods of section 3.

We now apply the propagation rules section 5.1 to the  $[[10, 3, 3]]$  code in figure 24 (right). The result of this procedure gives the same propagation as we found in figure 15 (left), because all we have changed is the arrangement of the parity check qubits which

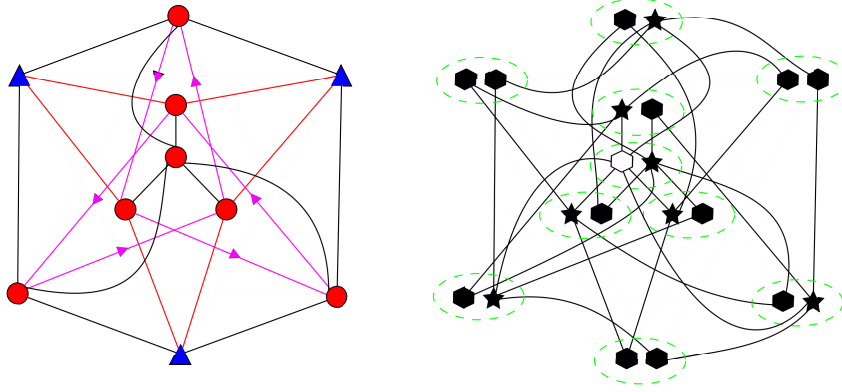


Figure 25: Left: Propagation rules applied to the  $[[10, 3, 3]]$  code in figure 24 (right). Right: Resulting classical code, green circles indicate classical bits created from the same qubits and are included as guides for they eye. Hexagons represent effective bits being checked for errors, and stars represent parity checks. Unfilled hexagons indicate parity check qubits which do not share any CNOTs with data qubits and therefore do not need to be corrected because they cannot propagate errors to the data.

check other parity check qubits. The result of applying these propagation rules can be seen in figure 25 (left), and the resultant classical code can be seen in figure 25 (right)

These more general quantum parity codes can also be represented as matrices. We represent the edges which connect the data qubits and the parity check qubits as two binary matrices, one for each type of edge. We call the matrix representing CNOTs which check for bit errors  $M^{(B^*)}$ , and the matrix which represents the conjugate controlled-Z gates which check for phase errors  $M^{(P^*)}$ . Each of these matrices will play the same role as  $M^{(B)}$  and  $M^{(P)}$  did in section 3.1, but must be larger to accommodate the possibility that *any* parity check qubit can check bit or phase information. The cross checks will be represented by the matrix  $M^{(C^*)}$ . Because cross checks can occur between *any* two parity check qubits, each side of this matrix must have a length equal to the number of parity check qubits. However, because  $M^{(C^*)}$  is an adjacency matrix with only one type of edge, we can constrain it to be upper triangular without loss of generality.

**Matrix Representations:** For the  $[[11, 3, 3]]$  and  $[[10, 3, 3]]$  quantum parity codes considered in this section, both will have  $M^{(B)}$  and  $M^{(P)}$  as given in equation (30). For the  $[[11, 3, 3]]$  code depicted in figure 24 (left), we have

$$M^{(B^*)} = \begin{pmatrix} 1 & 0 & 1 & 0 & 0 & 0 & 0 & 0 \\ 1 & 1 & 0 & 0 & 0 & 0 & 0 & 0 \\ 0 & 1 & 1 & 0 & 0 & 0 & 0 & 0 \end{pmatrix}$$

$$M^{(P^*)} = \begin{pmatrix} 0 & 0 & 0 & 0 & 1 & 0 & 1 & 0 \\ 0 & 0 & 0 & 0 & 1 & 1 & 0 & 0 \\ 0 & 0 & 0 & 0 & 0 & 1 & 1 & 0 \end{pmatrix}$$

$$M^{(C^*)} = \begin{pmatrix} 0 & 0 & 0 & 0 & 0 & 0 & 1 & 1 \\ 0 & 0 & 0 & 0 & 1 & 0 & 0 & 1 \\ 0 & 0 & 0 & 0 & 0 & 1 & 0 & 1 \\ 0 & 0 & 0 & 0 & 1 & 1 & 1 & 1 \\ 0 & 0 & 0 & 0 & 0 & 0 & 0 & 0 \\ 0 & 0 & 0 & 0 & 0 & 0 & 0 & 0 \\ 0 & 0 & 0 & 0 & 0 & 0 & 0 & 0 \\ 0 & 0 & 0 & 0 & 0 & 0 & 0 & 0 \end{pmatrix}, \quad (32)$$

where blue colouring indicates elements which have to be zero in the less general formalism. The  $[[10, 3, 3]]$  code has matrices

$$\begin{aligned} M^{(B^*)} &= \begin{pmatrix} 1 & 0 & 1 & 0 & 0 & 0 & 0 \\ 1 & 1 & 0 & 0 & 0 & 0 & 0 \\ 0 & 1 & 1 & 0 & 0 & 0 & 0 \end{pmatrix} \\ M^{(P^*)} &= \begin{pmatrix} 0 & 0 & 0 & 1 & 0 & 1 & 0 \\ 0 & 0 & 0 & 1 & 1 & 0 & 0 \\ 0 & 0 & 0 & 0 & 1 & 1 & 0 \end{pmatrix} \\ M^{(C^*)} &= \begin{pmatrix} 0 & 0 & 0 & 0 & 0 & 1 & 1 \\ 0 & 0 & 0 & 1 & 0 & 0 & 1 \\ 0 & 0 & 0 & 0 & 1 & 0 & 1 \\ 0 & 0 & 0 & 0 & 0 & 0 & 1 \\ 0 & 0 & 0 & 0 & 0 & 0 & 1 \\ 0 & 0 & 0 & 0 & 0 & 0 & 1 \\ 0 & 0 & 0 & 0 & 0 & 0 & 0 \end{pmatrix}. \end{aligned} \quad (33)$$

### 5.3 Proof of the more general graphical formalism

The proof of the more general graphical formalism follows much the same format as the one given in section 3.3. For all but the self loops, we consider a circuit transformation through which all checks which are directed to a given parity check qubit occur before all other checks. As before, causality prevents the gates directed to the other parity check qubits from having any effect on the state of that qubit. To do this we must consider two commutation relationships. Firstly, conjugate controlled-Z gates, which we write as  $\widetilde{\text{CZ}}(i, j)$  will always commute with each other. Note that this gate is symmetric, so we don't need to specify 'target' or 'control'.

$$[\widetilde{\text{CZ}}(i, j), \widetilde{\text{CZ}}(k, l)] = 0. \quad (34)$$

Secondly, we need the commutation relation between these gates and CNOTs,

$$[\widetilde{\text{CZ}}(i, j), \text{CNOT}(k, l)] = \delta_{j,l}(1 - \delta_{i,k}) \widetilde{\text{CZ}}(i, k) + \delta_{i,k} \delta_{j,l} U''(j, k) + i \longleftrightarrow j, \quad (35)$$

where  $U''(j, k)$  is a unitary operator the exact form of which is not required for this discussion and  $i \longleftrightarrow j$  indicates the previous expression but with  $i$  and  $j$  swapped. From these relationships, it is clear that for each qubit, the cross terms generated from error propagation will be the same as observed previously in section 3.3, with phase checks

occurring on a data qubit prior to bit-flip checks generating cross check terms, as is expressed graphically by the arrows between different parity check bits.

However, the more general construction admits a new possibility, that a phase check can be followed by a bit check on the same data qubit and going to the same parity check qubit. This is represented graphically by self loops. Moreover, because both checks are performed by the same parity check qubit, we cannot use an appeal to causality. Fortunately, it is straightforward demonstrate directly that a phase error will be translated into a bit error. Let us consider a single data qubit and a single parity check qubit in the initial state

$$|\psi\rangle \otimes |0\rangle = a |00\rangle + b |10\rangle,$$

we now apply a CNOT and  $\widetilde{CZ}$  to the qubits and arrive at the state

$$\frac{a}{\sqrt{2}}(|0+\rangle + |1-\rangle) + \frac{b}{\sqrt{2}}(|0+\rangle - |1-\rangle)$$

where  $|+\rangle = \frac{|1\rangle+|0\rangle}{\sqrt{2}}$  and  $|-\rangle = \frac{|1\rangle-|0\rangle}{\sqrt{2}}$ . We apply a phase flip to the parity check qubit,

$$\frac{a}{\sqrt{2}}(|0-\rangle + |1+\rangle) + \frac{b}{\sqrt{2}}(|0-\rangle - |1+\rangle).$$

Finally, the result of performing a  $\widetilde{CZ}$  followed by a CNOT to decode is

$$a |11\rangle + b |01\rangle = (X |\psi\rangle) \otimes |1\rangle,$$

demonstrating that a phase error does indeed propagate to a detectable bit-flip on the same parity qubit, as the graphical formalism shows. It is straightforward to show by the same method that no extra propagation, beyond what would be expected from the CNOT and  $\widetilde{CZ}$  being performed on two different data qubits, occurs for any other types of errors – this is left as “an exercise for the reader”.

## 6 CPC codes and stabilizer codes

We saw in section 2.4 that a coherent parity check effectively puts the joint system of data+parity check qubits into an eigenstate of a known operator. We can extend this to a stabilizer description for all codes constructed using CPC methods. Not only are able to give the effective stabilizer operators that can be seen as being measured in the code, but we can also identify the logical operators for the individual logical qubits within the code. This enables us to find a significant connection between CPC-constructed codes and CSS codes.

### 6.1 Stabilizers for separable CPC codes

The stabilizer measured when a phase parity check qubit is measured is determined by the matrices  $M^{(P)}$  and  $M^{(C)}$ , which determine the  $X$  stabilizers which are gathered by each of these qubits. Each of these stabilizers is

$$S_i^{(P)} = X_{p_i} \prod_{j=1}^{|d|} X_{d_j}^{M_{ji}^{(P)}} \prod_{k=1}^{|b|} X_{b_k}^{M_{ki}^{(C)}}. \quad (36)$$

where  $d$  is the set of data qubits,  $p$  is the set of phase parity check qubits, and  $b$  is the set of bit-flip parity check qubits.

For the stabilizers which the bit parity check qubits measure ( $Z$  stabilizers), one must additionally keep track of propagation from the phase check parity qubits to the bit-flip check parity qubits, as depicted by the magenta arrows in figure 9. The equation for these stabilizers is

$$S_i^{(B)} = Z_{b_i} \prod_{j=1}^{|d|} Z_{d_j}^{M_{ji}^{(B)}} \prod_{k=1}^{|p|} Z_{p_k}^{M_{ik}^{(C)}} \prod_{l=1}^{|p|} Z_{p_l}^{\sum_q M_{ql}^{(P)} M_{qi}^{(B)}}, \quad (37)$$

For the  $[[11,3,3]]$  code, it is possible to ‘brute force’ calculate the set of stabilizers, and to check that it matches these equations. Starting in a state where each of the four bit-check qubits, indexed by  $b_i$ , is initialised in  $|0\rangle$  and each phase-check qubit, given by  $p_j$ , is in  $|+\rangle$ , then with the three data qubit states (for simplicity)  $|d_i\rangle = |+\rangle$  the action of the encoder on the stabilizers is

$$\begin{array}{l} Z_{b_1} \\ Z_{b_2} \\ Z_{b_3} \\ Z_{b_4} \\ X_{p_1} \\ X_{p_2} \\ X_{p_3} \\ X_{p_4} \\ \hline X_{d_1} \\ X_{d_2} \\ X_{d_3} \end{array} \longrightarrow \begin{array}{l} Z_{d_1} Z_{d_2} Z_{b_1} Z_{p_2} Z_{p_4} \\ Z_{d_2} Z_{d_3} Z_{b_2} Z_{p_3} Z_{p_4} \\ Z_{d_1} Z_{d_3} Z_{b_3} Z_{p_1} Z_{p_4} \\ Z_{b_4} Z_{p_1} Z_{p_2} Z_{p_3} Z_{p_4} \\ X_{d_1} X_{d_2} X_{b_2} X_{b_4} X_{p_1} \\ X_{d_2} X_{d_3} X_{b_3} X_{b_4} X_{p_2} \\ X_{d_1} X_{d_3} X_{b_1} X_{b_4} X_{p_3} \\ X_{b_1} X_{b_2} X_{b_3} X_{b_4} X_{p_4} \\ \hline X_{d_1} X_{b_1} X_{b_3} \\ X_{d_2} X_{b_1} X_{b_2} \\ X_{d_3} X_{b_2} X_{b_3} \end{array}$$

The stabilizers above the line are those corresponding the operator measured after subsequent operations. These do not, as we can see, change depending on the state of the data qubits. They match the equations (36) and (37). Below the line we have the logical stabilizers. We chose to start in this case with each of the three qubits in memory in a pure stabilizer state. In general, this will not be the case, and the full set of stabilizers will be convex combinations of this and the different  $X$ -operator parities. That need not concern us here. What is useful from this choice, however, is that the three operators below the line on the RHS are now the logical  $X$  operators for the three encoded logical qubits. We see explicitly that this is a distance 3 code (the length of these operators). Furthermore, there is the interesting property that the logical operators overlap – each bit-check parity qubit is involved in two logical operators. We find similar for the logical  $Z$  operators and the phase-check parity qubits.

There is an important point to note about the distribution of the support of these logical operators. The CPC construction means that the  $X$  and  $Z$  logical operators spread out only onto the bit- and phase-check qubits that interact with them directly. The cross-checks, given by the matrix  $M^{(C)}$ , do not further delocalise the logical operator. We therefore have a (quasi-)local structure for the logical operators. Rather than each logical qubit being diffused across the whole space, it is restricted to local regions, each of which overlap at the edges. This structure can be viewed as a kind of half-way house between the

complete separation of logical spaces found in many topological codes, and the situation in many CSS codes where the distribution of the logical operators across supporting qubits has no simple graphical interpretation, being almost entirely delocalised.

## 6.2 Stabilizers in the More General Formalism

Finally, as with the less general formalism discussed above, the measured stabilizers for the more general formalism can also be derived from the matrix which gives the code. The formula is:

$$S_i = Z_{c_i} \prod_{j=1}^{|d|} Z_{d_j}^{M_{ji}^{(B^*)}} \prod_{j=1}^{|d|} X_{d_j}^{M_{ji}^{(P^*)}} \prod_{j=1}^{|c|} X_{c_j}^{(M_{ji}^{(C^*)} + M_{ij}^{(C^*)} + \sum_k M_{kj}^{(P^*)} M_{ki}^{(B^*)})} \quad (38)$$

where  $c$  is the set of parity check bits. It is straightforward to verify that if the code is in a split form, where the matrix elements indicated by blue colouring in Eq. 32 are zero, than by performing a Hadamard ( $Z \leftrightarrow X$ ) on the phase check parity bits, one recovers Eqs. 37 and 36.

## 6.3 Relationship to CSS codes

It was noted in section 2.4 that another way to understand coherent parity checks is the storing of mutual parity information about data qubits in the parity check qubits. For example, in the  $[[11,3,3]]$  code the mutual bit-parity information of the data qubits  $d_1, d_2$  is stored in the first bit-parity qubit  $b_1$ , along with that of the phase-check qubits  $p_2, p_4$ . This makes the system be in the known  $+1$  eigenstate of the operator  $Z_{d_1} Z_{d_2} Z_{b_1} Z_{p_2} Z_{p_4}$ , the first of the set of stabilizers given above. This is the same for all of the parity check qubits: for each  $b_i(p_i)$  there is a stabilizer containing only  $Z(X)$  components, and each  $b_i(p_i)$  is a member of only one such stabilizer. In the non-continuously encoded situation (where the qubits are effectively decoded and then re-encoded at each round of error correction), these stabilizers are the ones measured when the corresponding parity check qubit is measured after the unencoding step.

By construction then, every split CPC code can be written as a set of stabilizers where half contain only  $X$ s and half only  $Z$  operators. Furthermore, these can be divided into two sets, one containing stabilizers that vary depending on the encoded information (equal to the number of data qubits), and one containing known stabilizers, equal to the number of bit plus phase parity qubits. The latter set can be viewed as the generators of the code.

We can now compare CPC and CSS codes. A set of generators for a stabiliser subgroup (up to signs) can be written in symplectic notation as a matrix of the form:

$$G = (G_Z | G_X) \quad (39)$$

where  $G$  and  $G'$  are binary matrices where the  $(i, j)$ -th entry tells you whether a  $Z$  or an  $X$  is applied (for  $G_Z$  and  $G_X$  respectively) to the  $j$ -th qubit of the  $i$ -th stabiliser (?). In this form, standard CSS codes are written

$$G_{CSS} = \left( \begin{array}{c|c} G_Z & 0 \\ \hline 0 & G_X \end{array} \right) \quad (40)$$

For example, for the Steane  $[[7,1,3]]$  code,  $G_{X,Z}$  are both the parity check matrix of the classical  $[7,4,3]$  Hamming code.

For any CPC code, it is always possible to find a generating set of stabilizers such that the conditions we found above for the  $[[11,3,3]]$  code hold: that each bit(phase) parity check qubit appears in only one element of  $G_Z(G_X)$ . Using our previously-discussed matrices for bit, phase, and cross checks for CPC codes,  $M^{(B)}, M^{(P)}, M^{(C)}$ , the full set of stabilizers is then

$$G_{CPC} = \left( \begin{array}{ccc|ccc} (M^{(B)})^T & I & K & 0 & 0 & 0 \\ 0 & 0 & 0 & (M^{(P)})^T & M^{(C)} & I \end{array} \right) \quad (41)$$

where  $K := (M^{(C)})^T + (M^{(P)})^T M^{(B)}$  is the unique ‘‘correction’’ matrix which makes the induced stabilisers commute.

We can conclude two things immediately. First, CPC codes are CSS codes – and *vice versa*. That is, for any CSS code:

$$G_{CSS} = \left( \begin{array}{c|c} G_Z & 0 \\ 0 & G_X \end{array} \right) \quad (42)$$

we can perform Gauss-Jordan elimination (and possibly re-shuffle some columns) to obtain a new set of generators of the form:

$$G_{CSS} = \left( \begin{array}{ccc|ccc} G'_Z & I & G''_Z & 0 & 0 & 0 \\ 0 & 0 & 0 & G'_X & G''_X & I \end{array} \right) \quad (43)$$

Then, letting  $M^{(B)} := (G'_Z)^T$ ,  $M^{(P)} := (G'_X)^T$ , and  $M^{(C)} := G''_X$ , we obtain the equivalent CPC code.

For any CSS code, it will be possible to find a set of generators that allow identification of ‘bit parity qubits’ and ‘phase parity qubits’ in what is usually taken as an undifferentiated set of register qubits. With this identification in mind, CPC codes inherit all the properties of CSS codes.

Secondly, and more importantly, the CPC framework gives a method by which CSS codes can be constructed from known classical codes that differs significantly from the usual CSS framework. Classical codes have previously had to be carefully chosen for CSS codes so that the generators will commute. This is one reason why the framework is non-constructive: there is no way to start from a favourite classical code and turn it into a quantum one. Codes must be selected with care and simply tested to see if the generators commute. By contrast, in the CPC construction we can start from *any* classical code and create a quantum one. From (41) we see how to do this. Essentially, take classical parity check matrices as  $M^{(B)}$  and  $M^{(P)}$ , the cross-checks to ensure parity qubits are checked,  $M^{(C)}$ , and then finally apply the ‘‘correction’’  $(M^{(B)})^T M^{(P)}$  to ensure that the stabilisers commute.

As an example, consider again the standard CSS  $[[7,1,3]]$  code formed from two copies of the classical  $[7,4,3]$  code. We can use instead the CPC construction to create a different code based on the  $[7,4,3]$ . The classical parity check matrix is then both  $M^{(B)}$  and  $M^{(P)}$ ,

and by producing the cross-check matrix we construct the Hamming-based code of §4. This is a  $[[12,4,3]]$  code, more efficient than the  $[[7,1,3]]$  per logical qubit. By starting from the same classical code, the CPC construction produces CSS codes that are significantly more informationally dense than those given by the standard CSS construction, and furthermore enables *any* classical code to be used as the base for a quantum one.

## 7 Continuous protection for quantum memories

The working examples of quantum parity codes presented in the previous section are suitable as they stand for a quantum memory in which data qubits need to be kept fully coherent while storing quantum information. Quantum operations applied to these qubits need to be very fast and accurate compared with the memory storage times. As figure 16 shows, there are times during the encoding and decoding operations when the codes do not protect the data. On many hardware types, such as ion traps, CNOTs can be implemented very fast. This may not be true for other devices, and therefore it is desirable to design a code which can correct errors at arbitrary times rather than just during a specific time window. We will now extend our results to provide codes that protect data qubits continuously.

### 7.1 Protecting during encode and decode

As a first step towards this goal, we generate codes which do not have a ‘gap’ during which the qubits are unprotected. To construct such an implementation, let us first consider two copies of the CNOT sequence depicted in figure 9 performed sequentially on a set of data qubits, but with distinct sets of bit-flip check parity qubits and phase check parity qubits. To construct these codes, we commute sets of CNOTs through each other using Eq. 29, to arrive first at a circuit structure which maintains constant entanglement between the data bits and the bit and phase qubits as depicted in Fig. 27. We then further derive a circuit structure for which any bit or phase error which will be propagated to the data qubits will be detected in at least one measurement. It is important to note that this derivation is based only on the commutation structure of the CNOT matrices and is independent of the specific code which the circuit implements as well as the number of bit-flip and phase check qubits.

The first circuit transformation we perform to achieve this goal is to perform CNOTs pairwise in which the second set of phase check parity qubits act as controls on the first set of phase check parity bits, and likewise for the bit-flip check parity qubits, but with the second set of bits as the target as depicted in figure 26. Adding these CNOTs has no effect on the code because the action of a CNOT with a control initialized in the  $|0\rangle$  state is the identity, and likewise for a target initialized in the  $|+\rangle$  state.

To complete the ungapped code, the CNOTs used to initialize the bit and phase check parity qubits of the second parity code circuit are commuted through the pairwise CNOTs added in the previous transformation, after some cancellation the resultant circuit is the one depicted in figure 27. For bit-flip errors on the phase parity check bits, the set of CNOTs resulting from the commutator between the bit and phase CNOTs will have the same action as propagating to the data qubits and then to the bit-flip check qubits in

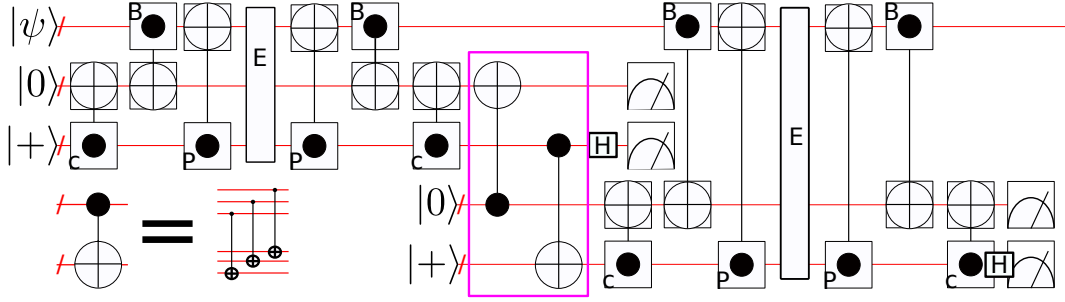


Figure 26: Two copies of the circuit pattern shown in 9 performed sequentially on the same data qubits, prepared in the collective state  $|\psi\rangle$  but with distinct bit-flip and phase check parity qubits. An additional set of CNOTs for which action is the identity because of the known state in which these qubits are initialized can be added as shown in the magenta box.

the circuit depicted in figure 9, therefore the graphical calculation methods of section 3.1 still remain valid, and the single error correcting codes given in section 4 will still correct all single qubit errors in the ungapped implementation.

While the fact that codes can be constructed which maintain constant entanglement with bit-flip and phase parity check qubits is encouraging for finding codes which can correct arbitrary errors rather than just those which occur within a fixed time window, it is not sufficient for this kind of correction. For instance, the phase error illustrated by a green  $z$  in figure 27 will propagate to the data qubits in an undetectable way as illustrated in by the green arrows. This error is propagated to the bit-flip parity check qubits, by the first set of cross check CNOTs, but than the detectable signal cancels itself out when it is propagated again by the second set of CNOTs.

It is worth pointing out that while naively it appears that ungapped codes double the required number of parity check qubits, this is not true, for the code in figure 27 assuming the number of bit-flip check parity qubits is at least as many as the number of phase check parity qubits, the measured qubits can be recycled for the second implementation, meaning that only one more qubit is required than for the gapped implementation.

The undetectable error propagation depicted by green arrows in figure 27 can be rectified by commuting the cross check CNOTs which occurs immediately after the the offending error through the pairwise CNOTs, resulting in the circuit depicted in figure 28. Except for the trivial cases of errors on the data bits before the initial encoding is complete or during the final decoding, errors occurring on any bits at any time which affect the data qubits are detectable.

Actually showing that error correction in the more general error model for which errors can occur at any time is possible would require explicitly checking every possible error in every possible position for a real code implemented with the circuit illustrated in figure 28. Such analysis is beyond the scope of this paper, but the fact that we can construct a circuit with no undetectable logical errors is suggestive that parity codes can be made compatible with a more general error model for which errors can occur at arbitrary times.

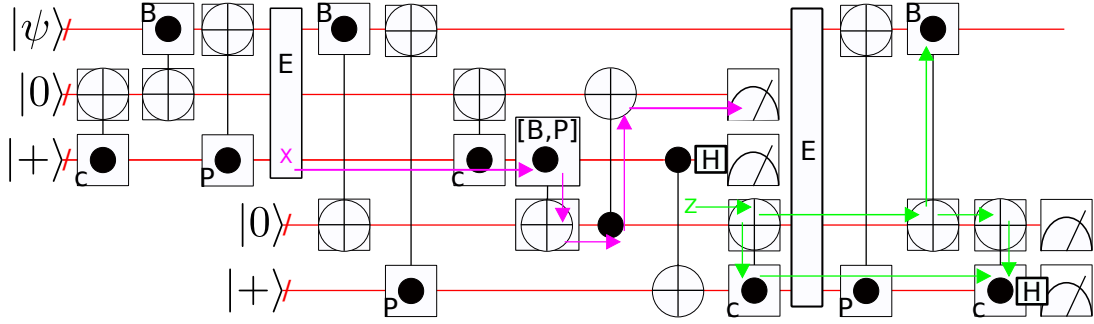


Figure 27: Ungapped circuit which maintains constant entanglement with parity check qubits. In this code the CNOTs in  $[B,P]$  are the product of the commutator between the two sets of CNOTs  $U^{[B,P]} = U^B U^P - U^P U^B$ . The magenta arrows show an indirect propagation path which propagates bit-flip errors on the phase check bits. The action of the commutator operator is the same as following the path illustrated in figure 9, therefore the analysis in Secs. 3.1 and 4. Green arrows illustrate that while a step in the right direction, this code cannot handle errors at arbitrary points, as exemplified by the propagation of an undetectable bit-flip error.

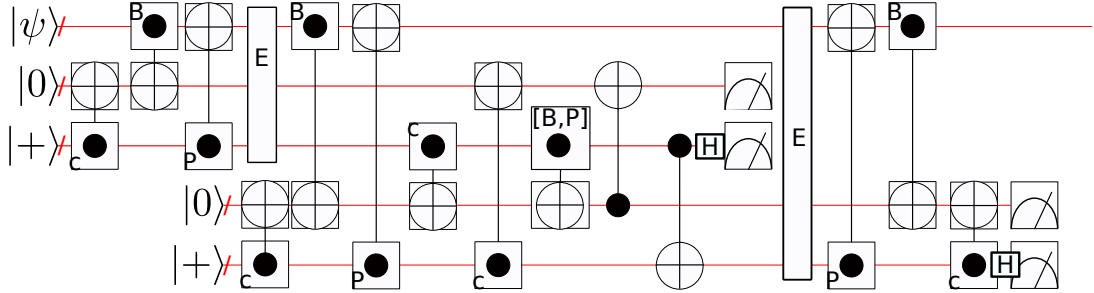


Figure 28: Ungapped circuit which maintains constant entanglement with parity check qubits, and allows detection of errors occurring at arbitrary times. In this code the CNOTs labelled  $[B,P]$  are the commutator between the two sets of CNOTs  $U^{[B,P]} = U^B U^P - U^P U^B$ , the controls and targets are found from the rules given in Eq. 29.

## 7.2 Asynchronous error checking

It is worth briefly pointing out that performing all CNOTs of one type (i.e. bit parity check, phase parity check, cross check etc...) together is not necessarily a natural strategy for a more general error model where errors can occur at any point. For this type of error, it is likely more desirable to refresh and measure one parity check qubit at a time. We refer to such codes as *asynchronous* parity codes. Decoding of such codes will necessarily be over time, and therefore more complicated. We will not consider these codes further in this paper, but they may provide a more natural setting for decoding with a more general error model for which errors can occur at any time.

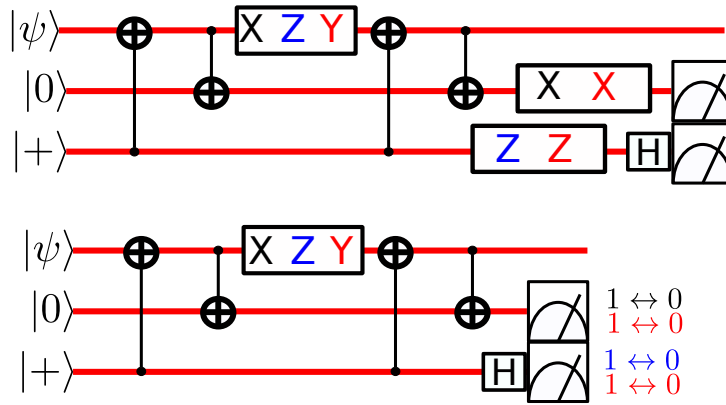


Figure 29: Different possible single logical Pauli operations, logical  $X$  is depicted in black while  $Z$  is in blue and  $Y$  in red. Top: explicit circuit including  $X$  and  $Y$  operations on the parity check qubits. Bottom: Circuit with  $X$  and  $Z$  operations on the parity check qubits replaced by classical post processing.

## 8 Computation encoded in error correction cycles

Having shown that quantum parity codes can be used to protect a quantum memory, and protect quantum data continuously while stored, the next logical step is to demonstrate that encoded computation is possible.

### 8.1 Single qubit operations

**Pauli Operations.** Applying a Pauli  $Z$ ,  $X$ , or  $Y$  operation, during the code cycle requires no change in the parity code circuit other than to apply the flip to the appropriate data qubit. The action of these gates is to perform a bit-flip ( $Z$ ), phase flip ( $X$ ) or both ( $Y$ ). These flips will propagate the same way in which errors do, and will have a predictable, deterministic effect on the measured parity check qubits. To see this, consider special cases of the circuit depicted in Fig. 29(top). In this case, the rotations performed on the parity check qubits will be  $X$  or  $Z$  operations. These operations however are equivalent to redefining the interpretation of the measured parity check bits so that  $1 \leftrightarrow 0$  for  $X$  and  $- \leftrightarrow +$  for  $Z$ , therefore other than the operation on the data qubit, no actual change of the circuit is required as the gates on the parity check qubits can be ‘effectively’ performed by appropriate post-processing as depicted in Fig. 29(bottom). The data qubits remain protected throughout, and should there be errors in the operations, they will be detected as normal after the post-processing is performed.

**Hadamard Gate.** The Hadamard gate cannot be encoded by simply changing the decoding strategy, it mixes information between the  $X$  and  $Z$  subspaces of a qubit, and therefore would lead to decoherence in the unaltered circuit. The way to implement a Hadamard can be determined by commuting the Hadamard operation through the encoder, thereby turning CNOTs for which the Hadamarded data qubit is the target into controlled- $Z$  gates, and those for which it is the control to a controlled  $Z$  acting in the conjugate basis as illustrated in figure 30. The Hadamard can thus be applied by

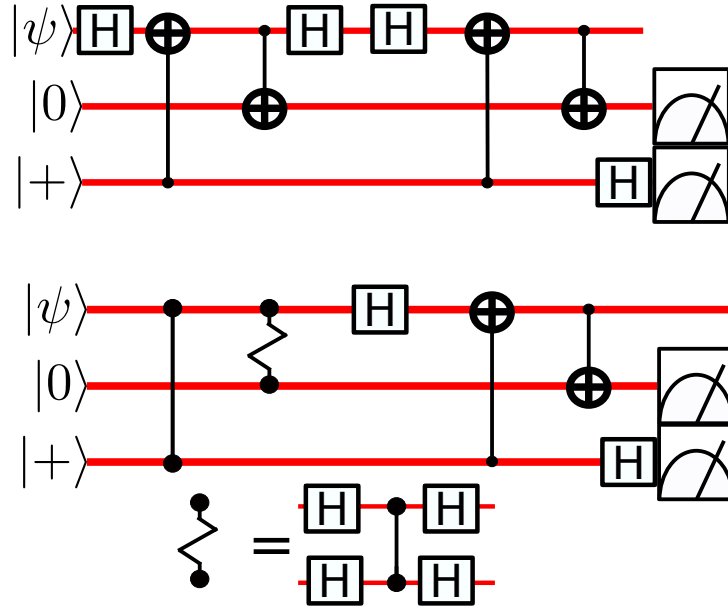


Figure 30: Top: Result of commuting a Hadamard gate into a parity code circuit showing only one of the phase check qubits and one of the bit-flip check qubits. Bottom: Equivalent circuit with Hadamards absorbed into logical gates to turn CNOTs into controlled Z or a controlled Z acting in the conjugate basis.

performing a Hadamard on the appropriate data qubit and changing some of the CNOTs in the encoding part of the cycle, corresponding to the data qubit requiring the Hadamard operation. Compare this with the ancilla-mediated quantum gates in [Proctor and Kendon \(2016\)](#). Note that this gate could be incorporated into an ungapped code following the procedure of section 7. We expect this method can be extended for arbitrary single-qubit rotations.

## 8.2 Entangling gates: encoded cnot

Any entangling gate can be created from a composition of a CNOT and single qubit rotations. Thus, we only need to demonstrate an encoded CNOT to show that arbitrary entangling gates are possible on quantum parity encoded qubits. Performing a CNOT between two data qubits in a parity code changes the way in which information is propagated. In general, this would trigger error detection in the parity check qubit measurements. Moreover, it would also cause information about the state of the encoded qubits to be propagated to the measurements, thereby converting the parity code circuit into one which measures information about the state of the data qubits. Hence, it is necessary to change either the encoding or decoding circuit to compensate for the information which the CNOT will propagate.

To determine how to construct such an encoder, let us first imagine a CNOT which is performed before (after) the quantum parity code is implemented, and commuting it forward (backward) into the time period for which the parity code acts as a quantum memory. The resulting circuit is depicted in figure 31. The gapped CNOT embeddings illustrated in figure 31 can also be incorporated into an ungapped or even asynchronous

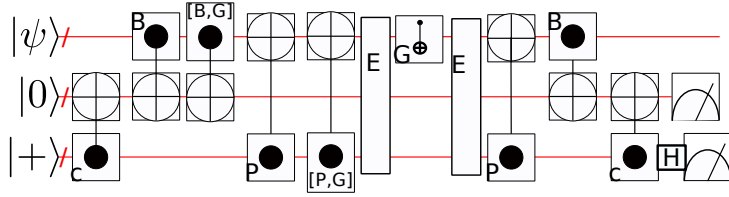


Figure 31: Strategy for encoding a CNOT into parity codes by Commuting a CNOT ( $G$ ) through the encoding circuitry to modify it to compensate for the generated entanglement. Note that  $[A, B]$  is the commutator between two sets of CNOTs  $U^{[A,B]} = U^A U^B - U^B U^A$ .  $G$  denotes the added CNOT between two data qubits.

code using the methods of section 7.

As figure 31 illustrates, for the encoded CNOT, we should consider both the possibility of an error happening before the CNOT as well as after, because the CNOT will propagate errors that happen before it. Considering the method of the top subfigure, a single bit-flip (phase) error before the control (target) of the CNOT becomes effectively two errors of the same type. If the underlying code is able to correct arbitrary two qubit errors, then the code will be able to correct this type of error. However, if not than this may introduce a single qubit error which is uncorrectable.

If the code is not able to correct arbitrary two qubit errors, it could still be made to correct the *specific* two qubit errors which are introduced by the CNOT. If we are able to find a code which generally only corrects single qubit errors, but also yields a unique signature for the two qubit errors propagated from the CNOT, then such a code will be able to implement a CNOT which is tolerant to all single qubit errors. Such a strategy could also be incorporated into ungapped codes. While the resultant circuit would be more complicated than the ones in section 7.1, there is no reason why the derivation which starts in figure 26 needs to have the same code within the first and second half of the code cycle, so long as the number of bit-flip and phase check qubits are the same. The circuit could be morphed into one which can handle the errors propagated to the CNOT for the cycle in which it occurs, and then morphed back.

**Randomly generated codes for encoded cnots.** We have been able to find codes through automated random searches which are able to correct single qubit errors as well as specific two qubit errors, such that they are compatible with the method depicted in figure 31. For a code which corrects single errors to be compatible with performing encoded CNOT operations, it must be able to correct pairs of errors propagated by the CNOT as well as all single qubit errors. To generate such codes, we have numerically tested randomly generated codes until we find one with a unique decoding for all relevant errors. We have found that this process works best if we enforce the constraint that the bit-flip and phase parity check matrices be the same, although we are not sure if there is a fundamental reason for this, or if it is a statistical artifact relating to this rather blunt numerical method.

For  $[[11, 3, 3]]$  codes,

$$M^{(B)} = \begin{pmatrix} 0 & 0 & 1 & 1 \\ 1 & 0 & 0 & 1 \\ 1 & 1 & 0 & 0 \end{pmatrix} \quad M^{(P)} = \begin{pmatrix} 0 & 0 & 1 & 1 \\ 1 & 0 & 0 & 1 \\ 1 & 1 & 0 & 0 \end{pmatrix} \quad M^{(C)} = \begin{pmatrix} 1 & 0 & 1 & 1 \\ 0 & 1 & 1 & 1 \\ 1 & 1 & 1 & 0 \\ 1 & 1 & 0 & 1 \end{pmatrix},$$

is compatible with performing a CNOT with the first data bit acting as the control and the second as the target. For  $[[12, 4, 3]]$  codes,

$$M^{(B)} = \begin{pmatrix} 0 & 0 & 1 & 1 \\ 0 & 1 & 0 & 1 \\ 1 & 0 & 0 & 1 \\ 1 & 1 & 0 & 1 \end{pmatrix} \quad M^{(P)} = \begin{pmatrix} 0 & 0 & 1 & 1 \\ 0 & 1 & 0 & 1 \\ 1 & 0 & 0 & 1 \\ 1 & 1 & 0 & 1 \end{pmatrix} \quad M^{(C)} = \begin{pmatrix} 1 & 0 & 1 & 0 \\ 1 & 0 & 1 & 1 \\ 1 & 1 & 1 & 0 \\ 0 & 1 & 1 & 1 \end{pmatrix}.$$

is similarly effective. We have found a significant number of other such codes, we include these two as examples. Given the ease of producing such codes, it is doubtful that publishing a long list would be beneficial to the community.

**Additional qubits checking encoded cnots.** Another method to compensate for the presence of two qubit errors propagated by encoded CNOTs is to introduce a pair of additional qubits, one which checks for bit-flips in the control qubit of the encoded CNOT and another which checks for phase errors in the target qubit. Mathematically, we add a row vector to the end of  $M^{(B)}$  which has a single non-zero element corresponding to the control (bit-flips) and another for the target. These qubits allow the cases for which an error may have been propagated by the CNOT to be checked separately from all single qubit errors on other qubits.

A code which can uniquely identify single qubit errors implies that the signature of a bit-flip (phase) error on just the control (target) of the CNOT must differ from the same type of error on both. This strategy will work as long as errors propagated from these additional qubits can also be uniquely detected. Codes like those in equation (26) and (31) have a qubit which checks only the other parity check qubits. These check checking qubits can be used to detect such propagating errors, by adding an additional CNOT between the two additional check qubits. This will flag this type of error as different from any on the original parity check qubits. Modifying our  $[[11, 3, 3]]$  code in this way to accommodate a CNOT between the first qubit (control) and the second (target) yields the following  $[[13, 3, 3]]$  code

$$M^{(B)} = \begin{pmatrix} 1 & 0 & 1 & 0 & \color{red}{1} \\ 1 & 1 & 0 & 0 & \color{red}{0} \\ 0 & 1 & 1 & 0 & \color{red}{0} \end{pmatrix} \quad M^{(P)} = \begin{pmatrix} 1 & 0 & 1 & 0 & \color{red}{0} \\ 1 & 1 & 0 & 0 & \color{red}{1} \\ 0 & 1 & 1 & 0 & \color{red}{0} \end{pmatrix} \quad M^{(C)} = \begin{pmatrix} 0 & 0 & 1 & 1 & \color{red}{0} \\ 1 & 0 & 0 & 1 & \color{red}{0} \\ 0 & 1 & 0 & 1 & \color{red}{0} \\ 1 & 1 & 1 & 1 & \color{red}{1} \\ \color{red}{0} & \color{red}{0} & \color{red}{0} & \color{red}{1} & \color{red}{1} \end{pmatrix}, \tag{44}$$

where coupling involving the additional qubits is shown in red.

### 8.3 Multiple operations per cycle

So far we have demonstrated how a single operation, either a CNOT or an arbitrary single qubit operation, may be encoded in a single error correction cycle of a parity code. However, depending on the error rates for different gates, it may be desirable to perform multiple operations in a single cycle. For single qubit operations, this is simple. One just needs to keep track of all (virtual) operations on all parity check qubits and compose them.

For multiple CNOTs, the circuit for encoding can be constructed by sequentially commuting CNOTs through the encoder circuit. However, for decoding one must be careful to make sure that all possible errors propagated through the CNOTs can be corrected. If multiple CNOTs are connected together in a chain (control of one before target of the other or vice versa), then a single error can propagate to appear as many errors.

It is also feasible to combine both CNOTs and single qubit operations in the same cycle, provided the propagation of the single qubit rotations through the encoded CNOTs is also accounted for.

## 9 Explicit calculation of CPC codes in Quantomatic

In this section, we will demonstrate the explicit calculation of stabilisers, error table, and encoded CNOT operation in the 3-qubit example using the Quantomatic tool [Kissinger and Zamdzhiev \(2015\)](#). Quantomatic is a tool for representing and transforming quantum circuits. In order to do this efficiently, it represents circuits using *ZX notation*, which we will now introduce briefly. Quantomatic is available from:

<http://quantomatic.github.io>

To give a flavour for these calculations, we will work with the  $[[11, 3, 3]]$  code from the introduction to this paper in this section, computing its single-qubit error table and an encoded CNOT. The full Quantomatic project used here is available from here:

<https://github.com/Quantomatic/cpc>

Quantomatic projects can be furthermore be exported as interactive web pages. For a fully-explicit calculation of a CNOT-compatible  $[[12, 4, 3]]$ , visit:

<http://quantomatic.github.io/cpc/12-4.html>

### ZX-notation and the ZX-calculus

ZX-notation is a superset of the usual quantum circuit notation. It is used to depict linear maps from qubits to qubits, put together in the usual way via composition and tensor product. The only operations in ZX-notation are swap gates, identities, and special linear maps called *spiders*. These come in two varieties, Z-spiders depicted as green dots:

$$\begin{array}{c} \diagup \\ \vdots \\ \bullet \\ \vdots \\ \diagdown \end{array} := |0 \cdots 0\rangle\langle 0 \cdots 0| + e^{i\alpha} |1 \cdots 1\rangle\langle 1 \cdots 1|$$

and X-spiders depicted as red dots:

$$\begin{array}{c} \diagup \\ \vdots \\ \bullet \\ \vdots \\ \diagdown \end{array} := |+\dots+\rangle\langle+\dots+| + e^{i\alpha}|-\dots-\rangle\langle-\dots-|$$

A special case is when spiders have a single input and output, in which case they form Z-phase and X-phase gates:

$$\text{---} \bullet \text{---} = |0\rangle\langle 0| + e^{i\alpha}|1\rangle\langle 1| = Z_\alpha$$

and X-spiders depicted as red dots:

$$\text{---} \bullet \text{---} = |+\rangle\langle +| + e^{i\alpha}|-\rangle\langle -| = X_\alpha$$

Another special case is when  $\alpha = 0$ , in which case we omit the label:

$$\begin{array}{c} \diagup \\ \vdots \\ \bullet \\ \vdots \\ \diagdown \end{array} := |0\dots 0\rangle\langle 0\dots 0| + |1\dots 1\rangle\langle 1\dots 1|$$

$$\begin{array}{c} \diagup \\ \vdots \\ \bullet \\ \vdots \\ \diagdown \end{array} := |+\dots+\rangle\langle+\dots+| + |-\dots-\rangle\langle-\dots-|$$

These maps can be thought of as a generalisation of the GHZ state to a linear map. Indeed the Z-spider with 0 inputs and 3 outputs is the usual GHZ state (up to normalisation):

$$\begin{array}{c} \diagup \\ \vdots \\ \bullet \\ \vdots \\ \diagdown \end{array} = |000\rangle + |111\rangle$$

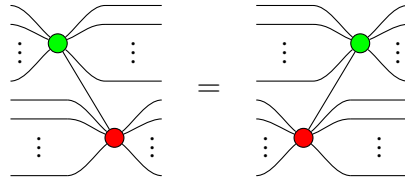
Furthermore, the  $|0\rangle$  and  $|+\rangle$  states are just one-legged spiders:

$$\bullet \text{---} = |0\rangle + |1\rangle \propto |+\rangle \quad \bullet \text{---} = |+\rangle + |-\rangle \propto |0\rangle$$

While spiders are typically non-unitary, and hence not quantum gates, they can be used to construct a universal family of quantum gates. We already saw Z- and X-phase gates, and the CNOT gate can be constructed as follows:

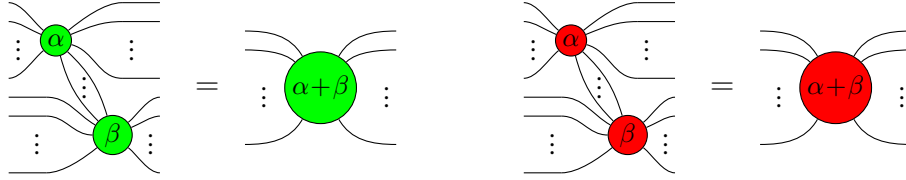


Note that we can write horizontal connections between spiders without ambiguity, because:

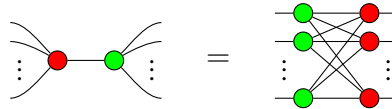


More generally, rather than treating a ZX-diagram as a (rigid) circuit consisting of spiders and swap gates, we can treat it as an undirected graph, again without ambiguity. That is, whenever two ZX-diagrams are isomorphic as undirected graphs, they describe the same linear operator.

Furthermore, ZX-notation admits a very useful set of rewrite rules, which are collectively referred to as the *ZX-calculus*. The ZX-calculus consists of 4 rules. The first two are the *spider-fusion* rules, which says adjacent spiders of the same colour fuse together, and their phases add:



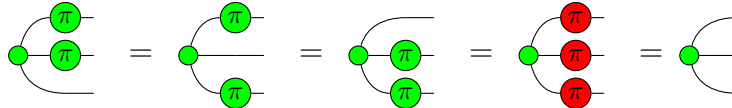
The third is the *spider-commutation* rule, which says a red spider connected by a single wire to a green spider (both with phase 0) can be replaced by a complete bipartite graph with the colours reversed:



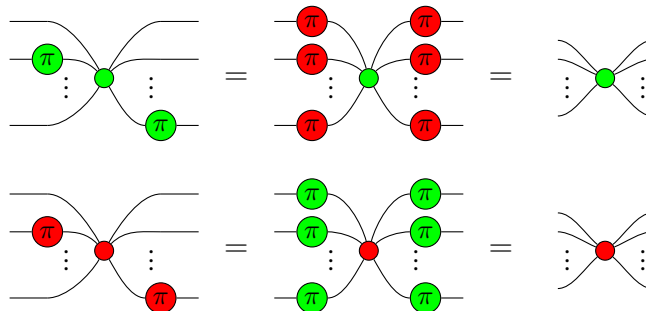
The fourth rule is the *Y-rule*, which gives the interaction between spiders and  $\frac{\pi}{2}$ -phase gates (a.k.a. *S-gates*):



Together, these four rules are *complete* for Clifford circuits [Backens \(2014\)](#). That is, if two Clifford circuits describe the same unitary, one can be rewritten into the other using the ZX-calculus. In particular, these rules imply the stabiliser rules for GHZ:



and their generalisation to arbitrary spiders:

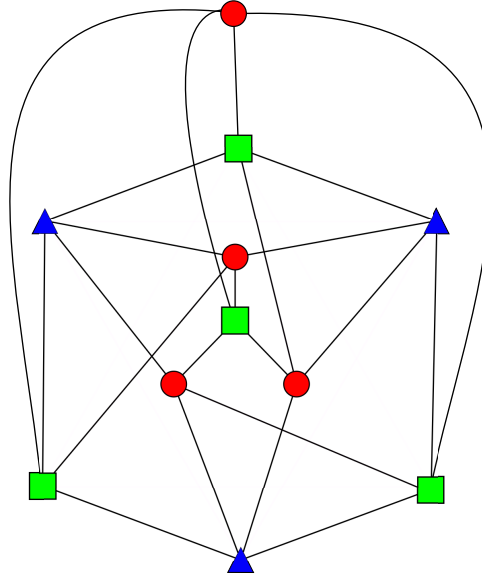


which make it very convenient for doing calculations involving stabiliser states and subspaces.

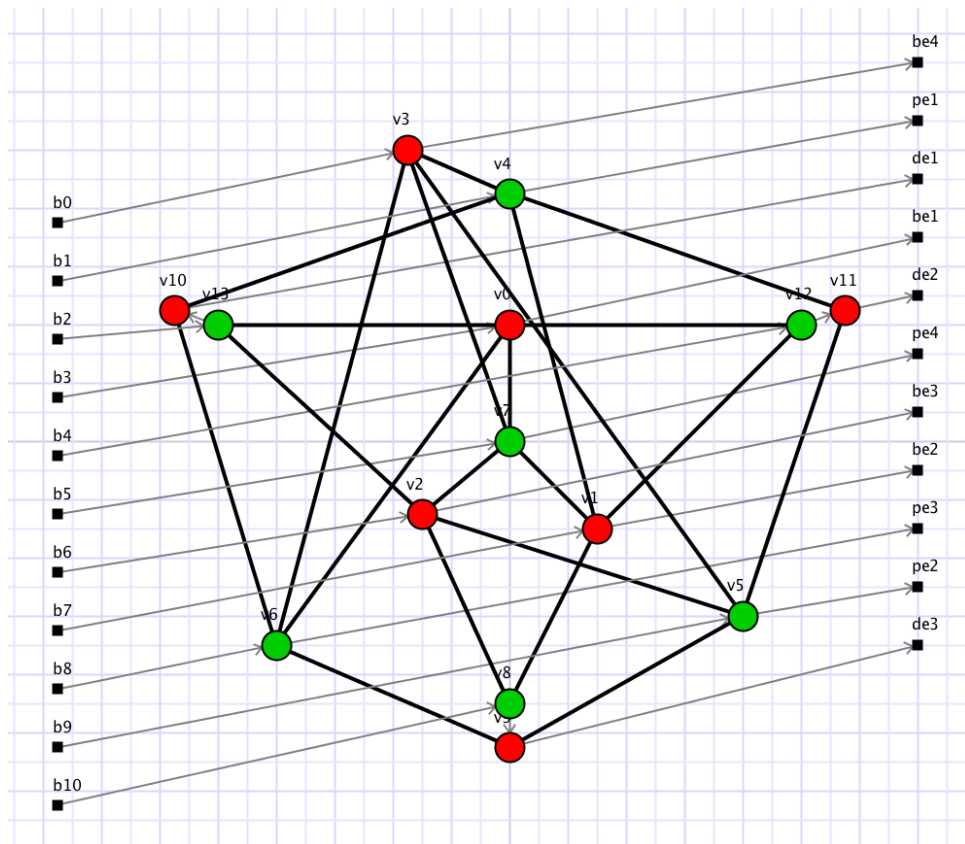
Quantomatic is a software tool for working with diagrams in ZX-notation using the ZX-calculus. For the remainder of this section, we will show how an  $[[11, 3, 3]]$  code and a  $[[12, 4, 3]]$  code can be expressed and verified in Quantomatic.

## Calculation of the $[[11, 3, 3]]$ code

We start with the  $[[11, 3, 3]]$  code, because it is easier to visualise. In fact, ZX-notation allows us to directly encode the graph-theoretic notation introduced in Section 3. For example, the code given in the introduction:



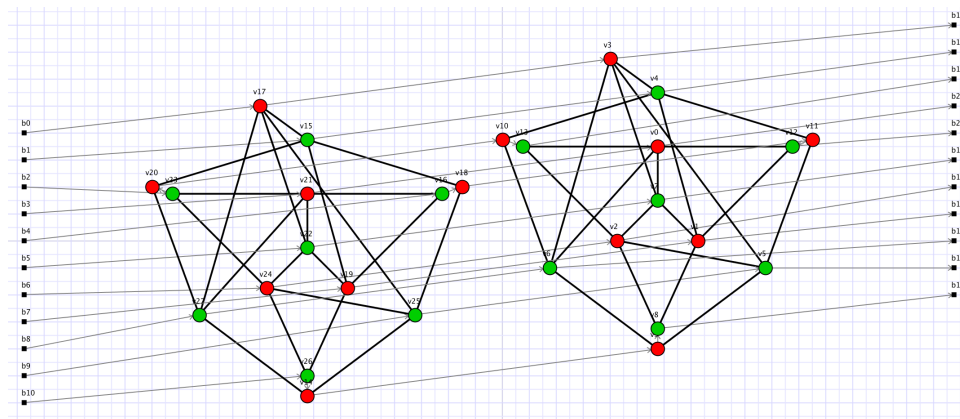
has a unitary encoding map, which can be expressed in ZX-notation as follows:



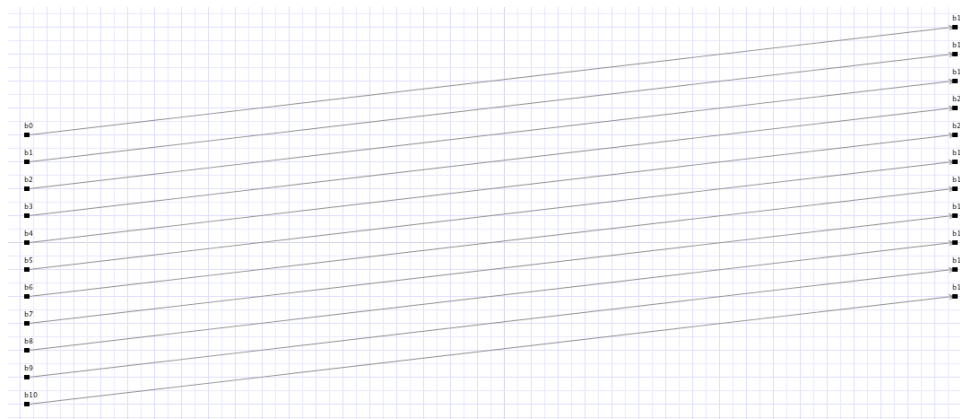
Red circles become red spiders and green squares become green spiders each with a single input and output (shown above as grey wires). Blue triangles become a pair consisting

of a green spider with an input connected to a red spider with an output. Edges between vertices become wires between spiders (shown above as bold black wires), subject to the rule that we always connect spiders of opposite colours in the case of edges to/from blue triangles.

The decoding unitary is constructed similarly, just reversing the role of inputs and outputs. Quantomatic can prove using the ZX-calculus that decoding indeed undoes encoding, namely that the following:

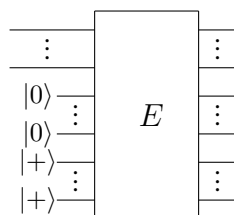


is equal to identity:

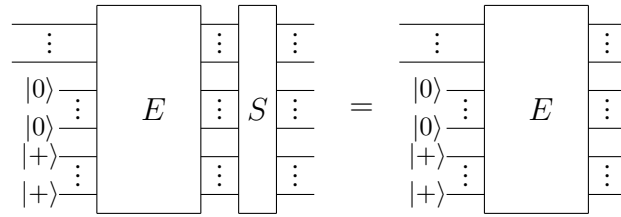


This can be solved automatically, using the `dir-simp` strategy in Quantomatic, which takes 50 steps (see Appendix).

Now, we can compute stabilisers for this code as follows. First, if we plug ancillas into the bit- and phase-check qubits, then only the data qubits remain as inputs. For an  $[[n, k, d]]$  code, this always gives us an isometry which embeds the  $k$ -qubit stabiliser subspace into  $n$ -qubit space:

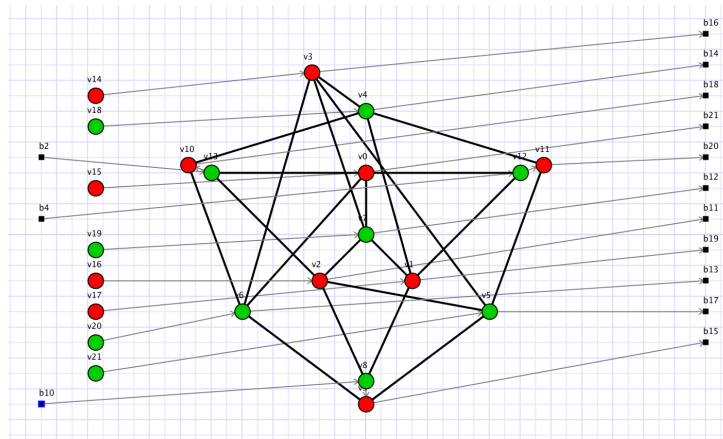


Then, to compute stabilisers of that subspace, we need to find elements of the Pauli group such that:

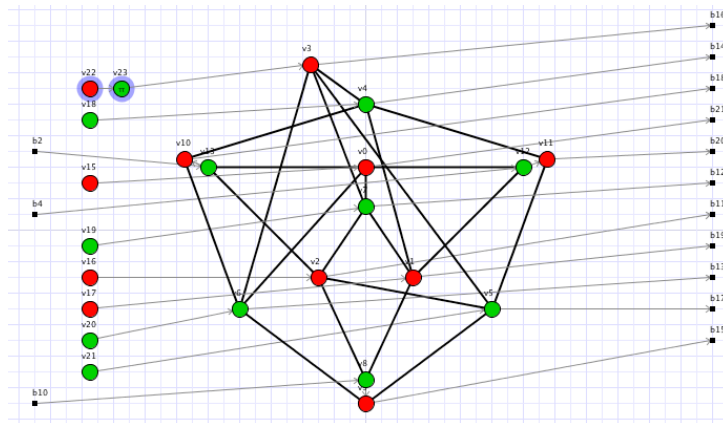


There are a number of ways to do this. Perhaps the simplest is the following. Since  $E$  is a Clifford circuit, we can always introduce a stabiliser on one of the ancillas via  $|0\rangle = Z|0\rangle$  or  $|+\rangle = X|+\rangle$ , then commute it through  $E$ . Since we have  $n - k$  ancillas, this will indeed give us  $n - k$  (independent) generators of the stabiliser group.

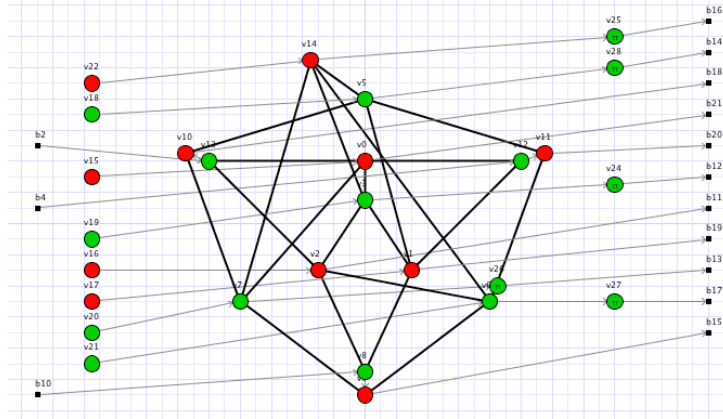
This can be done in Quantomatic as follows. First, we introduce ancillas on the parity-check qubits from our encoder:



then introduce a  $Z = Z_\pi$  on one of ancillas:



and push it through using the push strategy:



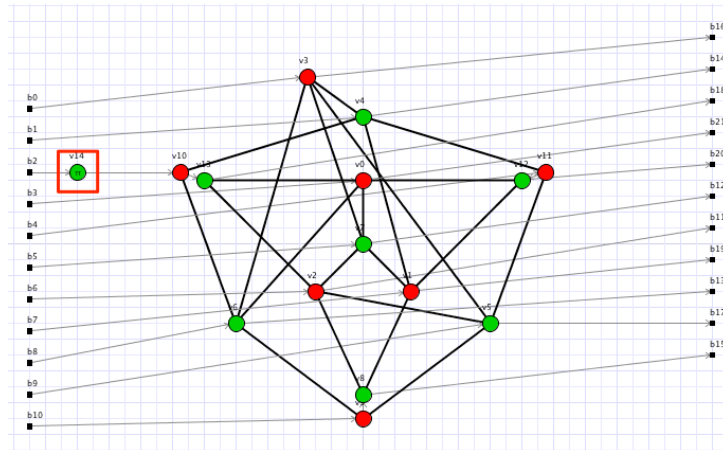
This takes 6 steps (see Appendix). If we repeat for all 8 ancillas, we obtain the following table:

### Stabilisers

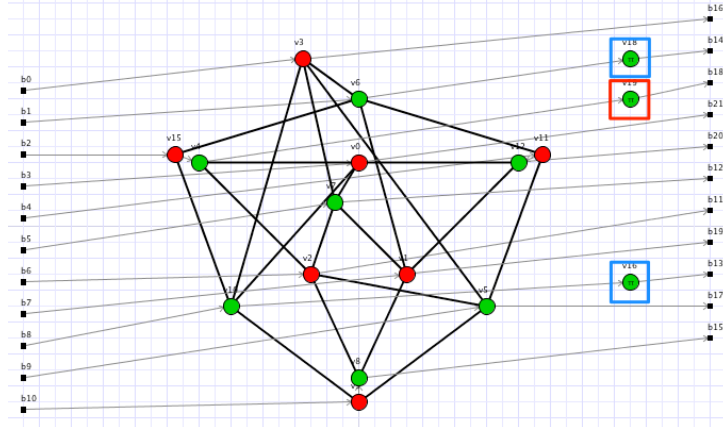
$$\begin{array}{c}
 \overline{Z_{d_1} Z_{d_2} Z_{b_1} Z_{p_2} Z_{p_4}} \\
 \overline{Z_{d_1} Z_{d_3} Z_{b_3} Z_{p_1} Z_{p_4}} \\
 \overline{Z_{d_2} Z_{d_3} Z_{b_2} Z_{p_3} Z_{p_4}} \\
 \overline{Z_{b_4} Z_{p_1} Z_{p_2} Z_{p_3} Z_{p_4}} \\
 \overline{X_{d_1} X_{d_2} X_{b_2} X_{b_4} X_{p_1}} \\
 \overline{X_{d_1} X_{d_3} X_{b_1} X_{b_4} X_{p_3}} \\
 \overline{X_{d_2} X_{d_3} X_{b_3} X_{b_4} X_{p_2}} \\
 \overline{X_{b_1} X_{b_2} X_{b_3} X_{b_4} X_{p_4}}
 \end{array}$$

which indeed matches the brute-force set of stabilizers obtained in section §6.

Calculating error tables is similar. We start by introducing a single-qubit error before the decoder:



and push it through using the push strategy:



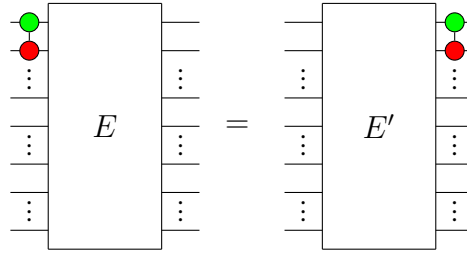
Then, a phase error on the first data qubit (shown in red) will register via error syndromes on two of the phase-check qubits (shown here in blue). A functional code then relies on the fact that each error syndrome corresponds to a unique combination of errors on the data qubits.

Quantomatic is Python-scriptable, so this can be done for all single-qubit errors via a small script (see Appendix). Inspection of the graphs produced yields the following error table:

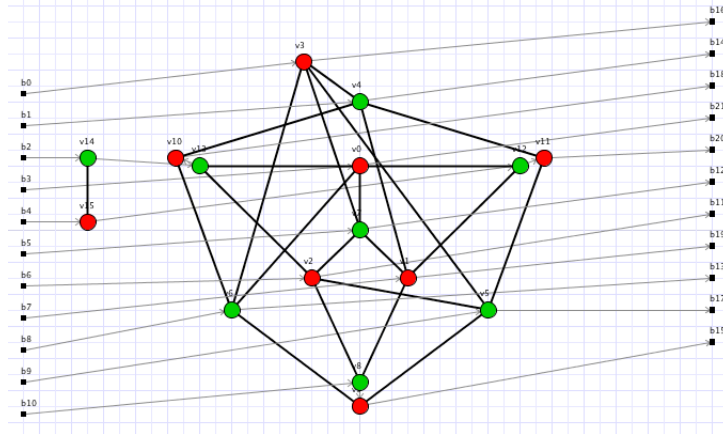
Error	Syndrome(s)
—	$X_{b_1}, X_{b_2}, X_{b_3}, X_{b_4},$ $X_{b_1}X_{b_2}X_{b_3}X_{b_4},$ $Z_{p_1}, Z_{p_2}, Z_{p_3}, Z_{p_4},$ $Z_{p_1}Z_{p_2}Z_{p_3}Z_{p_4}$
$X_{d_1}$	$X_{b_1}X_{b_3}$
$X_{d_2}$	$X_{b_1}X_{b_2}$
$X_{d_3}$	$X_{b_2}X_{b_3}$
$X_{d_1}X_{d_2}$	$X_{b_3}X_{b_4}$
$X_{d_1}X_{d_3}$	$X_{b_2}X_{b_4}$
$X_{d_2}X_{d_3}$	$X_{b_1}X_{b_4}$
$Z_{d_1}$	$Z_{p_1}Z_{p_3}$
$Z_{d_2}$	$Z_{p_1}Z_{p_2}$
$Z_{d_3}$	$Z_{p_2}Z_{p_3}$
$Z_{d_1}Z_{d_2}$	$Z_{p_3}Z_{p_4}$
$Z_{d_1}Z_{d_3}$	$Z_{p_2}Z_{p_4}$
$Z_{d_2}Z_{d_3}$	$Z_{p_1}Z_{p_4}$

which indeed yields a working code.

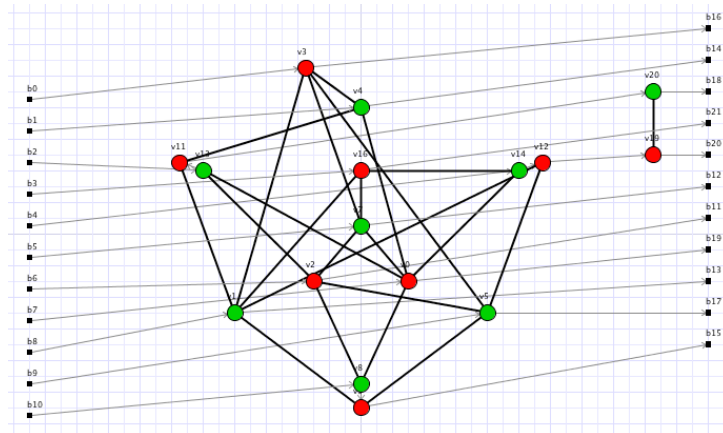
Finally, we conclude with a demonstration of encoded computation. Here, our goal is to perform a computation between the encoder and the decoder (i.e. in the error-corrected portion of the protocol) which has the same effect as performing a CNOT on the un-encoded qubits. This is accomplished by commuting the CNOT through the encoder, which causes the encoder to change:



In Quantomatic, we can perform this commutation using the ZX-calculus, to get from here:



to here:



This proof takes 18 steps (see Appendix).

## 10 Outlook and conclusions

There are some topics that are critical for repetition-code based quantum error correction that we have not yet touched on. Here we comment on a few, such as scaling, and thresholds, where the situation is very different for the codes constructed within the CPC framework.

## 10.1 Scaling for CPC codes

The examples we have demonstrated here are for small codes, however, it is generally understood in classical error correction that the performance of codes dramatically improves for larger codes. In fact, the Shannon limit can only be reached in the limit of code size approaching infinity. While it is not clear whether the structure of the parity codes constructed in the CPC formalism will allow them to approach the Shannon limit, it is likely that larger codes will perform better than smaller codes. This is in direct contrast to many quantum error correction models which are effectively based on repetition codes and derive no relative benefit from encoding more data qubits.

LDPCs are known to be state-of-the-art codes. This is both due to their performance close to the Shannon limit when their size becomes large, as well as due to the fact that there exist very fast (approximate) inference algorithms to decode them (cf. [MacKay \(2003\)](#)). It is thus important to see in how far those properties translate to our coherent parity code construction. Let us focus on the latter first. The main inference algorithm for LDPCs is based on belief propagation on graphical models. While such an algorithm is only exact for graphs which are trees, the algorithm is known to perform very well in practice for graphs which have not many small loops. Such properties can usually be achieved in practice. Furthermore, for given static codes and can also create decode tables. Our prime concern is thus the encoding level.

The main reason why LDPCs have such good performance is their large minimum code size. This is achieved through their random construction. In particular, for LDPCs the minimum code size scales linearly with the size of the code. The behaviour is essential to achieve performance which approaches the Shannon limit. Given the various constraints in the construction of our codes it is likely that for large codes one is not able to achieve minimum code which scales linearly. The situation would thus be similar to that of the quantum error correction codes derived in [MacKay et al. \(2004\)](#). However, as was shown in [MacKay et al. \(2004\)](#), as long as such a code has bounded code distance, they perform well in practice. Linearly growing minimal distance is formally only required when the noise level is taken to zero, for any small but finite noise level, a code with bounded distance will perform well in practice.

## 10.2 Thresholds

In the context of quantum error correction codes as they are traditionally formulated, the threshold, defined as the error rate for which the encoding propagates more errors than it corrects, is an important quantity. For such codes, encoding is always a losing strategy if the error rate is above the threshold. The threshold is especially important for families of codes where the threshold is independent of codes size, for example, toric codes.

For codes constructed within the CPC formalism, on the other hand, there is no reason to believe that for a given code, smaller codes which have the same threshold can be found. Therefore, while the threshold of any given code is a well defined mathematical quantity, an error rate being above the threshold of a code has no bearing on whether or not other codes can be found which can perform error correction at that error rate. The question of whether codes constructed in the CPC formalism can perform valid error correction at arbitrarily high error rates is open, but it cannot be answered by finding the threshold of individual codes.

### 10.3 Future directions

While in this work we focused on small codes related to LPDCs, the coherent parity code framework presented here can in principle be applied also to other codes, for example, turbo codes, which we already mentioned in the introduction, [Berrou et al. \(1993\)](#); [Berrou and Glavieux \(1996\)](#). Turbo codes are state-of-the-art codes which are for example used in 3G and 4G mobile transmissions. While turbo codes fall into the class of so-called convolutional codes, they are very closely related to LDPCs [MacKay \(2002\)](#), and it is expected that quantum error correction schemes based on turbo codes can be constructed using our coherent parity check formalism.

The CPC construction of codes marks a significant step forward for the use of quantum error correction on deployable hardware in both the immediate and longer terms. It allows informationally-dense codes to be constructed for memory, communication, and computation, either based on any previously known classical code, or directly without using such a code as a starting point. The suite of graphical and automated tools can be used by anyone without requiring a back-ground in quantum theory or quantum error correction.

This paves the way for software design tools for quantum computers that give codes for specific hardware layouts and specifications. We have demonstrated automated design based on random search, but more powerful design tools could be constructed using more sophisticated algorithms such as evolutionary algorithms or those within the Monte Carlo ‘family’ of techniques, such as simulated annealing or parallel tempering. The CPC formalism also enables high-performance classical codes to be imported for use on quantum devices, closing the gap between the tools that have been developed in classical computer science and the theoretical structures of quantum error correction.

## Acknowledgments

DH and NC were funded by the UK EPSRC grant EP/L022303/1. SZ was funded by Nokia Technologies, Lockheed Martin and the University of Oxford through the quantum Optimisation and Machine Learning (QuOpaL) project. The authors would like to thank Viv Kendon for many useful discussions and comments on the text. We would also like to thank Joschka Roffe for multiple critical readings of the paper, and Samson Abramsky, Niel de Beaudrap, Earl Campbell, Elham Kashefi, and Tim Proctor for useful discussions of various aspects of these codes, and an anonymous referee for constructive comments.

## Appendix: Quantomatic strategies and proofs

Quantomatic enables custom strategies using a simple cominator-type language based on ML. The two strategies used in the previous section were the the `dir-simp` strategy, which is designed specifically to simplify ZX-representations of circuits:

```
open RG_SimpUtil

val_simps = load_ruleset [
  "dir-rules/dir-hopf", "dir-rules/dir-hopf2", "dir-rules/dir-hopf3",
```

```

    "dir-rules/green-id", "dir-rules/red-id"
];

```

```

val spiders = load_ruleset [
    "dir-rules/green-sp-dir", "dir-rules/red-sp-dir",
    "dir-rules/green-sp-dir2", "dir-rules/red-sp-dir2"
];

```

```

val simproc = LOOP (REDUCE_ALL simps ++ REDUCE_ALL spiders);
register_simproc ("dir-simp", simproc);

```

and the push strategy, which ‘pushes’ Pauli operations through such representations:

```

open RG_SimpUtil

```

```

val simps = load_ruleset [
    "pushers/gg", "pushers/rr",
    "pushers/rgd", "pushers/grd",
    "pushers/ggd", "pushers/rrd",
    "pushers/ggu", "pushers/rru"
];

```

```

val simproc = REDUCE_ALL simps;
register_simproc ("push", simproc);

```

It is additionally Python-scriptable, which is useful when one wants to do multiple, automated derivations. Here is the script used to generate the error table from the previous section:

```

from quanto.util.Scripting import *

# load decoder circuit
dec = load_graph('11-3/decoder')

# load rules for pushing Pauli X and Z through a circuit
rules = map(load_rule, [
    'pushers/gg', 'pushers/rr',
    'pushers/rgd', 'pushers/grd',
    'pushers/ggd', 'pushers/rrd',
    'pushers/ggu', 'pushers/rru'])

# plug Pauli X or Z into every input of the decoder
# and use 'rules' to push it to the output

inputs = ['b' + str(i) for i in range(11)]
for error in ['X', 'Z']:
    p = load_graph('pushers/' + error)
    for inp in inputs:

```

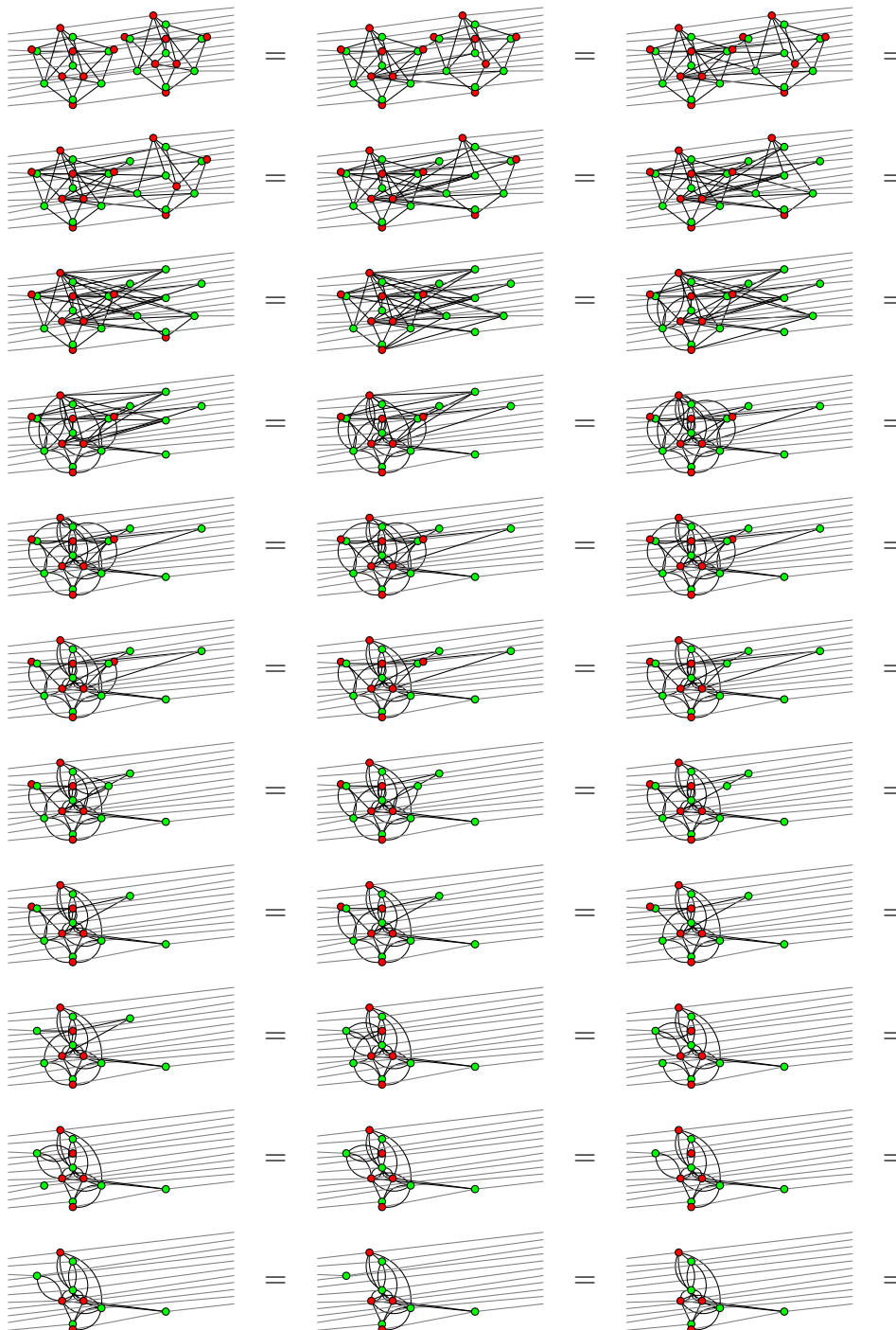
```

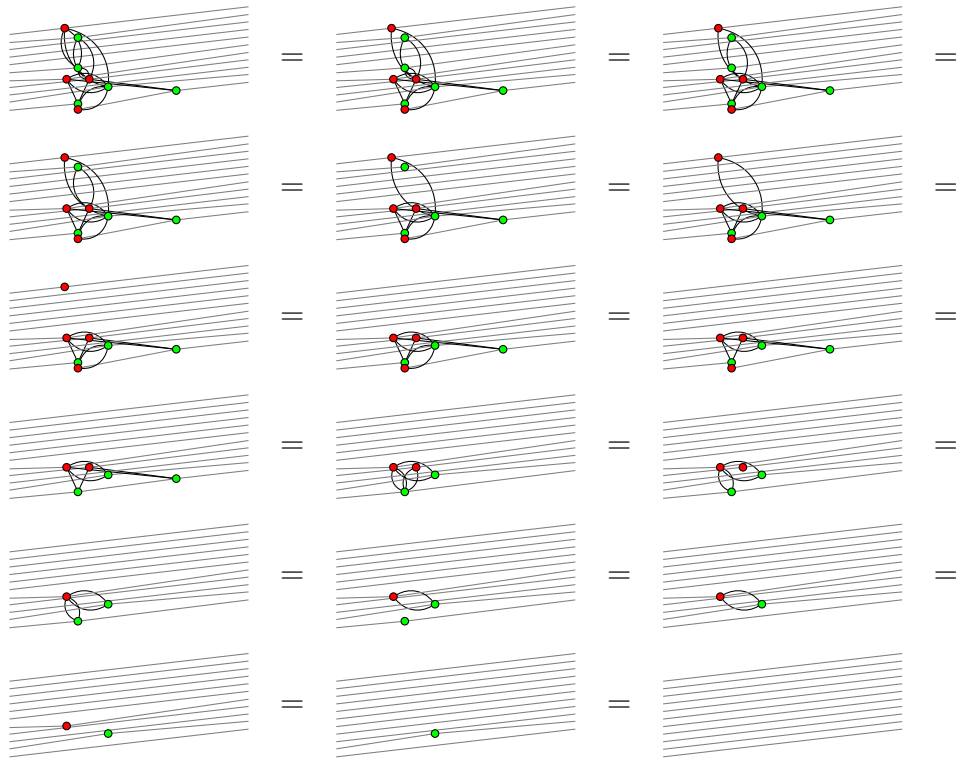
g = plug(dec, p, inp, 'b1')
d = derivation(g)
d.normalise(rules)
d.save('11-3/stab/error-' + error + '-' + inp)

```

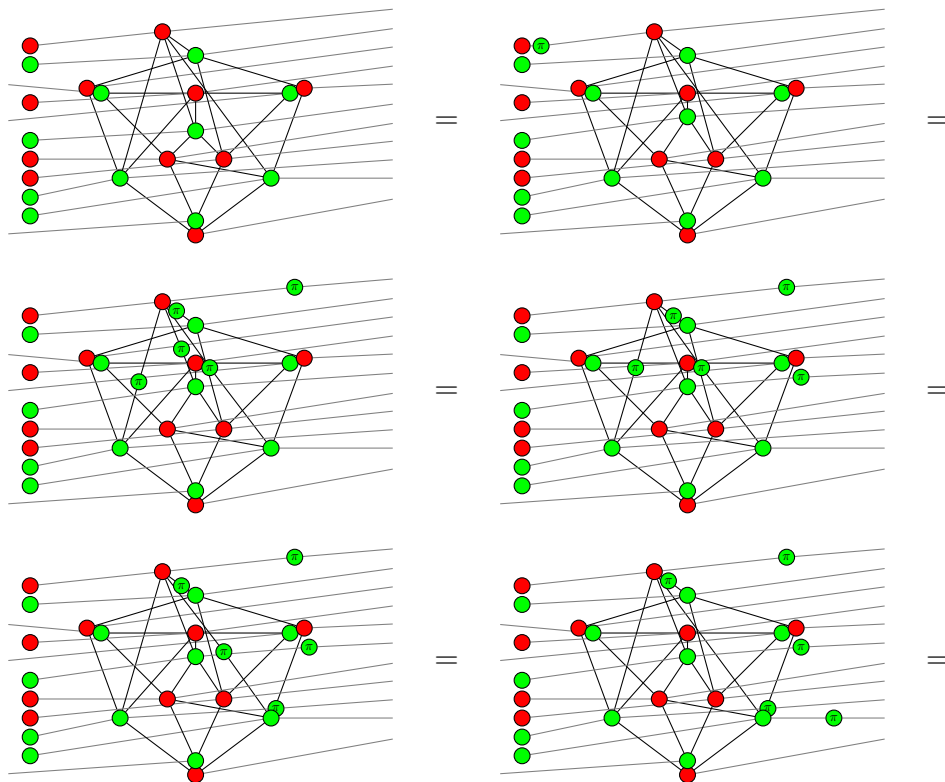
The script for computing stabilisers is very similar.

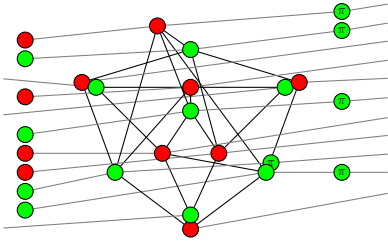
To give some idea of the scale and style of Quantomatic-generated proofs, we now provide a few samples of proofs used to verify the code from the previous section. The first is the proof that the  $[[11, 3, 3]]$  encode/decode is equal to identity:



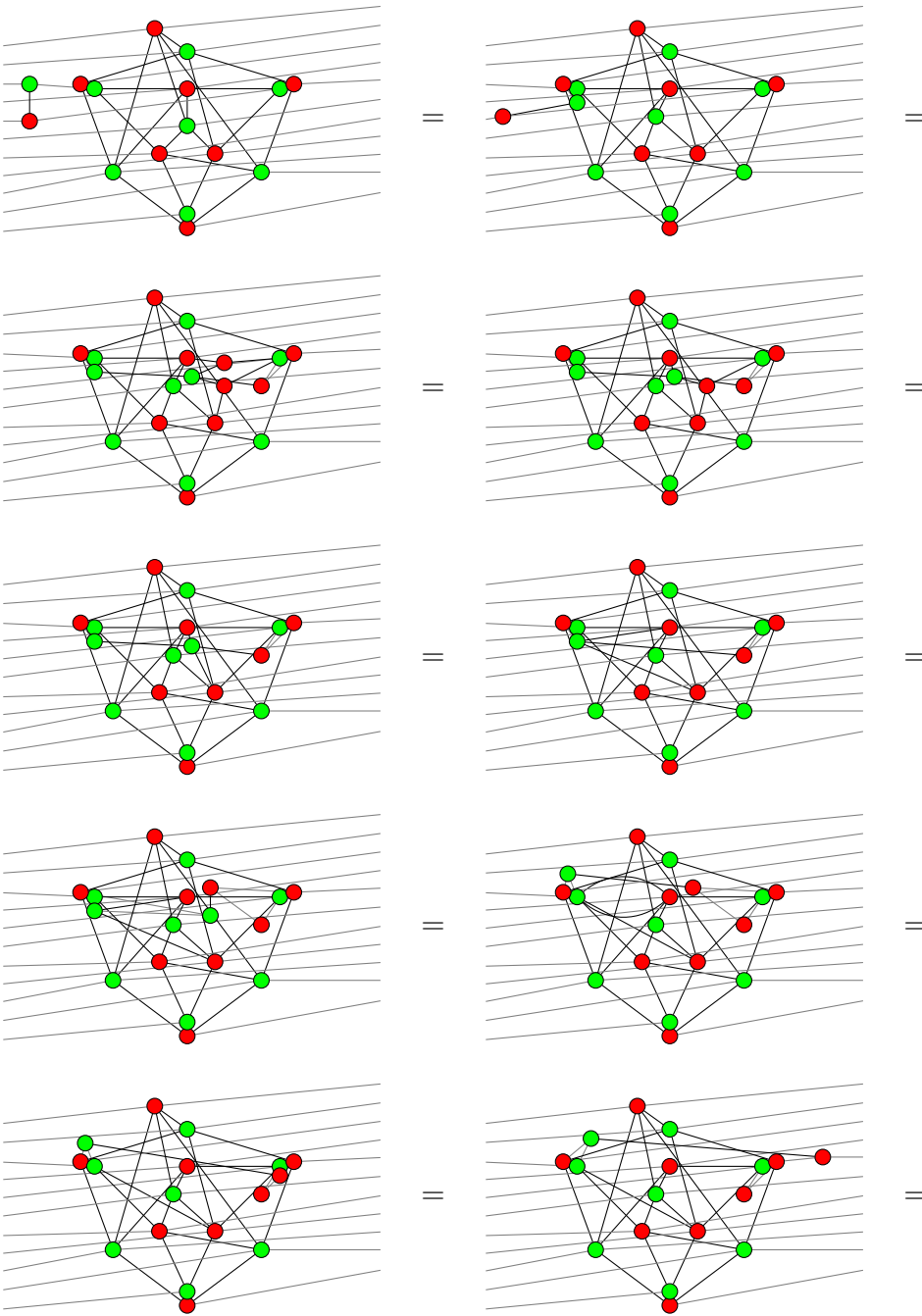


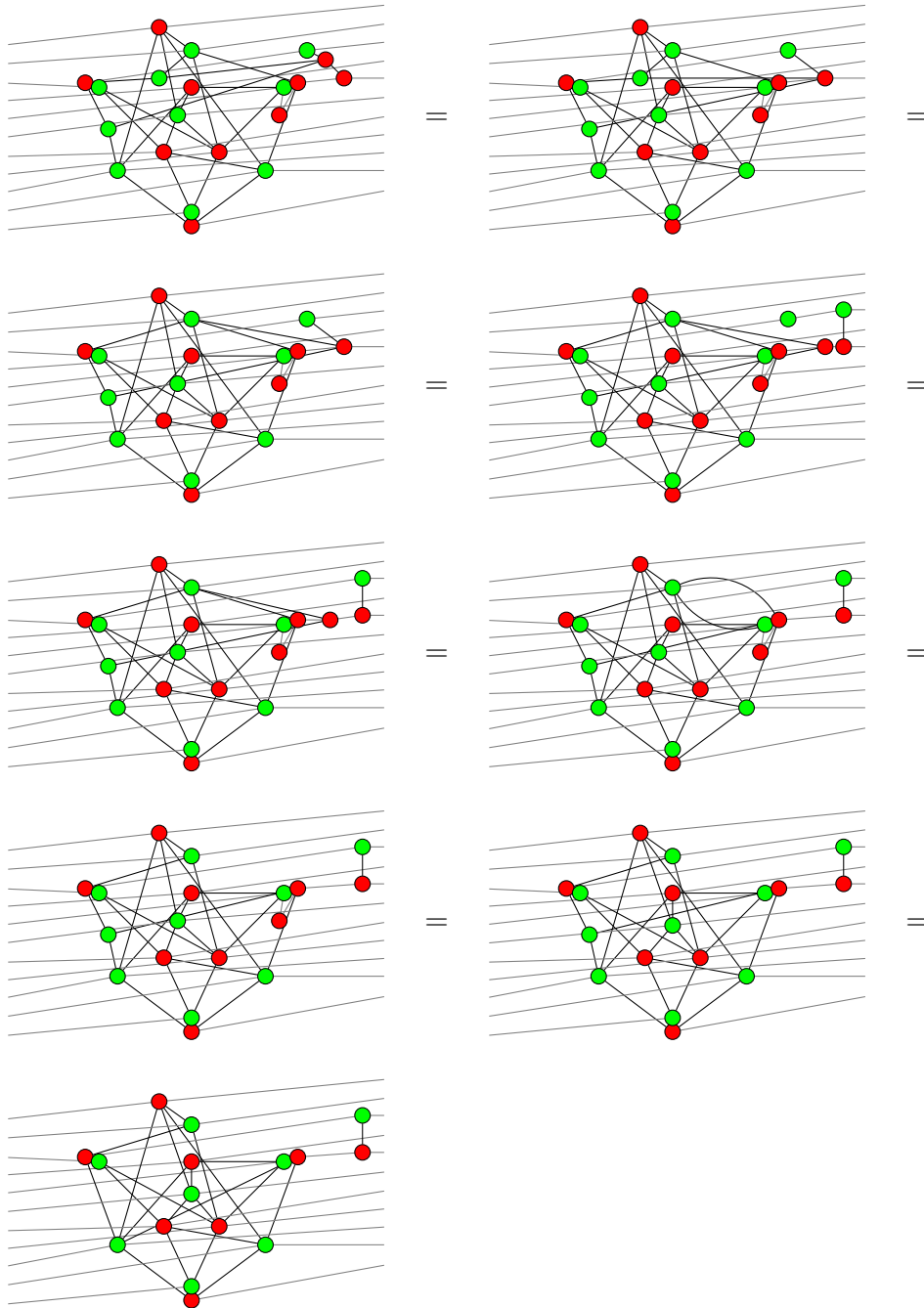
Next, the computation of the first stabiliser for the  $[[11, 3, 3]]$  code:





Finally, the computation of the modified encoder for an encoded CNOT:





## References

(n.d.). <http://www.research.ibm.com/quantum/>.

Aharonov, D. and Ben-Or, M. (1996). Fault tolerant quantum computation with constant error, *Proc. 29th ACM STOC*, ACM, NY, pp. 176–188. arXiv:quant-ph/9611025.

Anders, J., Oi, D. K. L., Kashefi, E., Browne, D. E. and Andersson, E. (2010). Ancilla-driven universal quantum computation, *Phys. Rev. A* **82**(2): 020301(R).

- Backens, M. (2014). The ZX-calculus is complete for stabilizer quantum mechanics, *New Journal of Physics* **16**: 093021. arXiv:1307.7025.
- Berrou, C. and Glavieux, A. (1996). Near optimum error correcting coding and decoding: Turbo-codes., *IEEE Trans. on Communications* **44**: 1261.
- Berrou, C., Glavieux, A. and Thitimajshima, P. (1993). Near shannon limit error-correcting coding and decoding: Turbo-codes., *Proc. 1993 IEEE International Conf. on Communications, Geneva, Switzerland*, p. 1064.
- Bian, Z. and et. al. (2014). Discrete optimization using quantum annealing on sparse ising models, *Frontiers in Physics* **2**: 00056.
- Bombin, H. and Martin-Delgado, M. (2008). Statistical mechanical models and topological color codes, *Physical Review A* **77**(4): 042322.
- Calderbank, A. R. and Shor, P. W. (1996). Good quantum error-correcting codes exist, *Phys. Rev. A* **54**: 1098–1106.
- Campbell, E. T. (2014). Enhanced fault-tolerant quantum computing in d-level systems, *Phys. Rev. Lett.* **113**(23): 1–5.
- Chancellor, N., Szoke, S., Vinci, W., Aeppli, G. and Warburton, P. A. (2016). Maximum-entropy inference with a programmable annealer, *Scientific Reports* **6**: 22318.
- Chancellor, N., Zohren, S. and Warburton, P. A. (2016). Circuit design for multi-body interactions in superconducting quantum annealing system with applications to a scalable architecture, arXiv:quant-ph:1603.09521.
- Chancellor, N., Zohren, S., Warburton, P. A., Benjamin, S. C. and Roberts, S. (2016). A direct mapping of max k-sat and high order parity checks to a chimera graph, arXiv:quant-ph:1604.00651.
- Dennis, E., Kitaev, A., Landahl, A. and Preskill, J. (2002). Topological quantum memory, *J. Math. Phys.* **43**: 4452.
- D-Wave Systems Inc. website* (2016). <http://www.dwavesys.com/>. Accessed: 2016-10-03.
- Easton, B. and Knill, E. (2009). Restrictions on transversal quantum gate sets, *Physical Review Letters* **102**(110502). arXiv:0811.4262 [quant-ph].
- Gallager, R. G. (1962). Low density parity check codes, *IRE Transactions on Information Theory* **8**(1): 21.
- Gallager, R. G. (1963). *Low Density Parity Check Codes*, number 21 in *MIT Research monograph series*, MIT Press.
- Gottesman, D. (2010). An introduction to quantum error correction and fault-tolerant quantum computation, *Proceedings of Symposia in Applied Mathematics*, Vol. 68. arXiv:0904.2557.

- Harty, T. P., Allcock, D., Ballance, C., Guidoni, L., Janacek, H., Linke, N., Stacey, D. and Lucas, D. (2014). High-fidelity preparation, gates, memory, and readout of a trapped-ion quantum bit, *Physical Review Letters* **113**: 220501.
- Inagaki, T., Inaba, K., Hamerly, R., Inoue, K., Yamamoto, Y. and Takesue, H. (2016). Large-scale ising spin network based on degenerate optical parametric oscillators, *Nature Photonics* **10**: 415–419.
- Kissinger, A. and Zamdzhiev, V. (2015). Quantomatic: A proof assistant for diagrammatic reasoning, *International Conference on Automated Deduction*, Springer, pp. 326–336.
- Kitaev, A. Y. (2003). Fault-tolerant quantum computation by anyons, *Annals of Physics* **303**.
- Knill, E., Laflamme, R. and Zurek, W. (1996). Threshold accuracy for quantum computation. ArXiv:quant-ph/9610011.
- Laflamme, R., Miquel, C., Paz, J. P. and Zurek, W. H. (1996). Perfect quantum error correcting code, *Phys. Rev. Lett.* **77**: 198–201.
- Leib, M., Zoller, P. and Lechner, W. (2016). A transmon quantum annealer: Decomposing many-body ising constraints into pair interactions, arXiv:1604.02359.
- MacKay, D. J. C. (1999). Good error correcting codes based on very sparse matrices, *IEEE Trans. on Info. Theory* **45**(2): 399.
- MacKay, D. J. C. (2002). Turbo codes are low density parity check codes, <http://www.inference.eng.cam.ac.uk/mackay/turbo-ldpc.pdf>.
- MacKay, D. J. C. (2003). *Information Theory, Inference, and Learning Algorithms*, Cambridge University Press.
- MacKay, D. J. C. and Neal, R. M. (1996). Near shannon limit performance of low density parity check codes., *Electronics Letters* **32**(18): 1645.
- MacKay, D. J., Mitchison, G. and McFadden, P. L. (2004). Sparse graph codes for quantum error-correction, *IEEE Transactions on Information Theory* **50**(10): 2315.
- Munro, W. J., Nemoto, K. and Spiller, T. P. (2005). Weak nonlinearities: a new route to optical quantum computation, *New J. Phys.* **7**(1): 137.
- Nickerson, N. H., Fitzsimons, J. F. and Benjamin, S. C. (2014). Freely scalable quantum technologies using cells of 5-to-50 qubits with very lossy and noisy photonic links, *Physical Review X* **4**(4): 041041.
- O’Malley, P. J. J., Babbush, R., Kivlichan, I. D., Romero, J., McClean, J. R., Barends, R., Kelly, J., Roushan, P., Tranter, A., Ding, N., Campbell, B., Chen, Y., Chen, Z., Chiaro, B., Dunsworth, A., Fowler, A. G., Jeffrey, E., Lucero, E., Megrant, A., Mutus, J. Y., Neeley, M., Neill, C., Quintana, C., Sank, D., Vainsencher, A., Wenner, J., White, T. C., Coveney, P. V., Love, P. J., Neven, H., Aspuru-Guzik, A. and Martinis, J. M.

- (2016). Scalable quantum simulation of molecular energies, *Phys. Rev. X* **6**: 031007.  
**URL:** <http://link.aps.org/doi/10.1103/PhysRevX.6.031007>
- Proctor, T. J. and Kendon, V. (2016). Hybrid quantum computing with ancillas, *Contemporary Physics* **57**.
- Raussendorf, R. and Harrington, J. (2007). Fault-tolerant quantum computation with high threshold in two dimensions, *Phys. Rev. Lett.* **98**: 190504.
- Raussendorf, R., Harrington, J. and Goyal, K. (2007). Topological fault-tolerance in cluster state quantum computation, *New J. Phys.* **9**(199).
- Rocchetto, A., Benjamin, S. C. and Li, Y. (2016). Stabilisers as a design tool for new forms of lechner-hauke-zoller annealer, arXiv:1603.08554.
- Shor, P. W. (1995). Scheme for reducing decoherence in quantum computer memory, *Phys. Rev. A* **52**: R2493.
- Steane, A. (1996a). Error correcting codes in quantum theory, *Phys. Rev. Lett.* **77**: 793–797.
- Steane, A. (1996b). Multiple particle interference and quantum error correction, *Proc. Roy. Soc. Lond. A* **452**: 2551. ArXiv:quant-ph/9601029.
- Yamaoka, M., Yoshimura, C., Hayashi, M., Okuyama, T., Aoki, H. and Mizuno, H. (2016). Advanced research into ai, ising computer, *Hitachi Review* **65**(6).